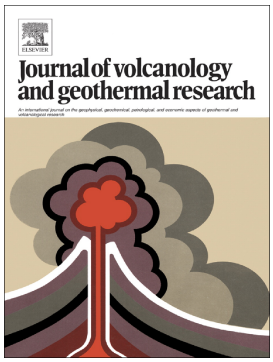

Seismicity during the recent activity (2009–2020) of Turrialba volcano, Costa Rica

Leonardo van der Laat, Mauricio M. Mora, Javier Fco. Pacheco, Philippe Lesage, Esteban Meneses

PII: S0377-0273(22)00182-2

DOI: https://doi.org/10.1016/j.jvolgeores.2022.107651

Reference: VOLGEO 107651

To appear in: *Journal of Volcanology and Geothermal Research*

Please cite this article as: L. van der Laat, M.M. Mora, J.F. Pacheco, et al., Seismicity during the recent activity (2009–2020) of Turrialba volcano, Costa Rica, *Journal of Volcanology and Geothermal Research* (2022), https://doi.org/10.1016/j.jvolgeores.2022.107651

- Turrialba volcano slowly transitioned from a closed- (2010) to an open-system (2017)
- Seismic tremor decreases precedes eruptive phases at Turrialba volcano
- Pre-eruptive tremor abatement is accompanied with SO_2 flux decrease
- Chromatic signals are common seismic precursors (e.g. tornillos, harmonic tremor)
- Magnitude 5.5 earthquake correlates with the transition to an open-vent system

Manuscript File

Declaration of interests

☒The authors declare that they have no known competing financial interests or personal relationships that could have appeared to influence the work reported in this paper.

☐The authors declare the following financial interests/personal relationships which may be considered as potential competing interests:

Seismicity during the recent activity (2009-2020) of Turrialba volcano, Costa Rica - Author Statement

August 15, 2022

Author contributions

Leonardo van der Laat: Conceptualization, Methodology, Software, Formal Analysis, Investigation, Writing - Original Draft, Visualization; **Mauricio Mora:** Supervision, Conceptualization, Methodology, Software, Formal Analysis, Investigation, Writing - Original Draft, Resources, Funding acquisition, Visualization **Javier Fco. Pacheco:** Supervision, Conceptualization, Resources, Formal Analysis, Investigation, Funding acquisition, **Philippe Lesage:** Formal Analysis, Writing - Review & Editing; **Esteban Meneses:** Writing - Review & Editing, Funding acquisition.

Supplementary Material

Seismicity during the recent activity (2009-2020) of Turrialba volcano, Costa Rica

Leonardo van der Laat[a,b,c,d,1,*], Mauricio M. Mora[b,c], Javier Fco. Pacheco[d], Philippe Lesage[e], Esteban Meneses[f]

[a]*Department of Earth and Environmental Sciences, University of Michigan, 1100 North University, Avenue, 4518 North University Building, Ann Arbor, MI 48109-1005*
[b]*Escuela Centroamericana de Geología, Universidad de Costa Rica, Apdo. 11501-2060, San José, Costa Rica*
[c]*Red Sismológica Nacional, Universidad de Costa Rica, Apdo. 11501-2060, San José, Costa Rica*
[d]*Observatorio Vulcanológico y Sismológico de Costa Rica, Universidad Nacional, Apdo. 2386-3000, Heredia, Costa Rica*
[e]*Université Grenoble Alpes, Université Savoie Mont Blanc, CNRS, IRD, Université Gustave Eiffel, ISTerre, 38000 Grenoble, France*
[f]*Colaboratorio Nacional de Computación Avanzada, Centro Nacional de Alta Tecnología, Apdo. 1174-1200, San José, Costa Rica*

Abstract

Turrialba is a stratovolcano located at the easternmost part of the Costa Rican volcanic front. After remaining quiescent for more than a century, in 1996 it started to show signs of unrest, until a first phreatomagmatic explosion occurred on January, 2010. Since then, the activity evolved from phreatic to magmatic, in a series of distinct eruptive phases. In this paper, we investigate the seismic records that span the whole eruptive process (2010-present), in order to identify precursory signals and characterize the volcanic evolution. A long-term analysis was carried out based on the continuous records, as well as seismic catalogs (volcano-tectonic seismicity, harmonic tremor, etc.). In addition, the gradual character of the evolution of this eruption allowed for the analysis of independent precursory stages. Thus, we inspected in detail the most important of those periods, particularly, prior to the first 2010 phreatomagmatic eruption, and prior to the 2016 transition to an open vent system. Temporary tremor amplitude decreases were found to precede most of the eruptive phases. In total, pre-eruptive tremor abatement periods were identified spanning several days (5-44), which often concurred with a decrease in the SO_2 flux. The analysis of the volcano-tectonic seismicity highlights the migration of magma from a deep (6-10 km) reservoir beneath the neighboring Irazú volcano towards Turrialba volcano, especially between the years 2015 and 2016. This activity peaked on December 2016 when a Mw 5.5 earthquake took place between both volcanoes. Harmonic tremor episodes thrived in the later phase when the system finally opened (2017-2018). In the short-term, compounded tonal seismic signals were identified as precursor events, such as long-period events followed by harmonic tremor or by a multichromatic coda similar to tornillo-type events. The co-occurrence of tremor amplitude decreases and tonal seismic signals is interpreted to be caused by a sealing of the hydrothermal system, which blocked the circulation of fluids and permitted the resonances in the inner cavities. This process leaded to pressure accumulation and the consequent eruptions. Thus, trough a series of cycles of sealing and rupture the system of conduits gradually opened. The seismic characterization of this eruption constitutes insightful knowledge useful for monitoring and risk assessment purposes.

Keywords: tremor, precursor, volcano, seismology, LP, tornillo

1. Introduction

Turrialba volcano is a (3,340 m a.s.l.) basaltic–andesitic stratovolcano located at the eastern edge of the Central Volcanic Range (CVR) of Costa Rica, 35 km east-northeast of San José, the capital and socioeconomic center of the

*Corresponding author
Email addresses: laat@umich.edu (Leonardo van der Laat), mauricio.mora@ucr.ac.cr (Mauricio M. Mora), javier.pacheco.alvarado@una.ac.cr (Javier Fco. Pacheco), lesage@univ-smb.fr (Philippe Lesage), emeneses@cenat.ac.cr (Esteban Meneses)
[1]Present address: Department of Earth and Environmental Sciences, University of Michigan, 1100 North University, Avenue, 4518 North University Building, Ann Arbor, MI 48109-1005

country. It is one of the five active volcanoes in Costa Rica and it has erupted with significance at least 10 times during the last 7,000 years (Reagan et al., 2006; Alvarado et al., 2020). The last major eruption took place between 1864 and 1866 and the volcano then remained quiescent for more than a century. In 1996, the volcano started to show signs of unrest that turned conspicuous in 2007 evidenced by geochemical changes in fumarole gas composition and increased seismicity (Hilton et al., 2010; Martini et al., 2010; Vaselli et al., 2010). The first phreatic eruptive phase occurred in January 5, 2010. Since then, the activity evolved from phreatic to magmatic, in a slow process of opening of conduits.

Understanding precursory seismicity at short and long terms is globally one of the major tasks in order to reduce volcanic risk. At Turrialba volcano, we were able to record part of the initial unrest before the first eruption in 2010 and all of the eruptive evolution towards the open-vent phase, this offers an important opportunity to understand seismic source processes at different stages of the volcanic activity of Turrialba.

In this work we focus on the precursory activity of the main eruptive stages at Turrialba volcano since 2010 up to 2020 by means of close inspection of seismic records with different time-frequency analysis, in order to understand the evolution of the eruption dynamics. We also carry out a detailed description and classification of Turrialba volcano seismicity. This is the first time that overall seismicity of Turrialba volcano is presented together with an interpretative model of the evolution of the system over the 11 years of activity.

1.1. Geological setting

Turrialba volcano, Costa Rica, is located in a complex geotectonic background where the Cocos, Caribbean, Nazca plates and the Panama microplate interact (Figure 1). The Cocos plate subducts beneath the Caribbean plate and the Panama microplate at an approximate rate of 90 mm/year (LaFemina et al., 2009). Subduction beneath Costa Rica is highly complex due to variations on the Cocos plate slab morphology and its petrological characteristics, but also because of its double interaction with the Caribbean plate and Panama microplate (Von Huene et al., 1995; Gazel et al., 2021). The southeastern portion of the Central American Volcanic Front (CAVF) in Costa Rica and Panama, developed on top of oceanic crust terranes, including the western edge of the Caribbean Large Igneous Province (CLIP) (Gazel et al., 2021). The oceanic crust subducting along northwestern Costa Rica was produced at the East Pacific Rise, while that beneath central Costa Rica and Panama was formed at the Cocos-Nazca spreading center and includes the 13.0–14.5 Ma Galapagos hotspot track (Von Huene et al., 1995; Werner et al., 1999; O'Connor et al., 2007). The subduction of the Cocos plate under the Caribbean plate generates profuse volcanism, resulting in the modern Costa Rica volcanic front (CRVF), that is oriented NW-SE and partitioned in three segments: at the NW the Guanacaste volcanic range (GVR), the Tilarán volcanic range (TVR) and to the SE the Central volcanic range (CVR). From NW to SE, the CVR comprises Platanar, Poás, Barva and Irazú-Turrialba volcanoes. Turrialba, in particular, is the only volcano that is shifted 10 km towards the NE from the CVR main axis.

Turrialba volcano lies on sedimentary deposits of the Limón Basin and its origin dates back to the Middle to Upper Pleistocene. Ruiz et al. (2010) and Soto (2012) consider three construction phases: 1) Proto-Turrialba that began around 1 Ma; 2) Paleo-Turrialba whose last phase corresponds to the Finca Liebres volcano (250 ka); and 3) Neo-Turrialba, the current phase. The lava and pyroclast compositions vary from basalt to dacite, being andesite and dacite the most important compositions (Ruiz et al., 2010; Soto, 2012). DeVitre et al. (2019) proposed that a multi-stage magma mixing occurred at Turrialba, starting at deep mid-crust reservoirs with a mingling between high-Nb decompression melt induced by corner-flow from the backarc and a low-Nb volcanic front component. A second stage resulted from the chaotic mixing at shallow reservoirs between the resulting basaltic andesite and the rhyolitic end-member, delivering the presumably differentiated residual magma from previous events such as that of 1864–1866.

Geophysical evidence suggests that the feeding system beneath Turrialba volcano is made up of two magma reservoirs. Conde et al. (2014) deduced two levels of magma storage from the clustering of localised seismic events, one probably at 4–6 km depth and the shallow one at roughly 1 km below the summit. de Moor et al. (2016), Müller (2018) and Badilla and Taylor (2019) proposed a mid-crust reservoir located in the range between 5-10 km, which is located beneath Irazú volcano according to Lücke et al. (2010) and Müller (2018). Di Piazza et al. (2019) also interpreted a deep magma reservoir (~13 km deep) for the andesitic magma involved in the ~2 ka sub-Plinian El Retiro eruption. A second, shallower and smaller, reservoir could be in the range 1-2 km (de Moor et al., 2016; Badilla and Taylor, 2019).

Tectonic faults cutting Turrialba volcanic structure are characterized by left (NE-SW) and right-lateral (SW-NE) strike-slip systems (Soto, 1988; Montero et al., 2013; Calvo et al., 2019) (Figure 2). Turrialba volcano has three

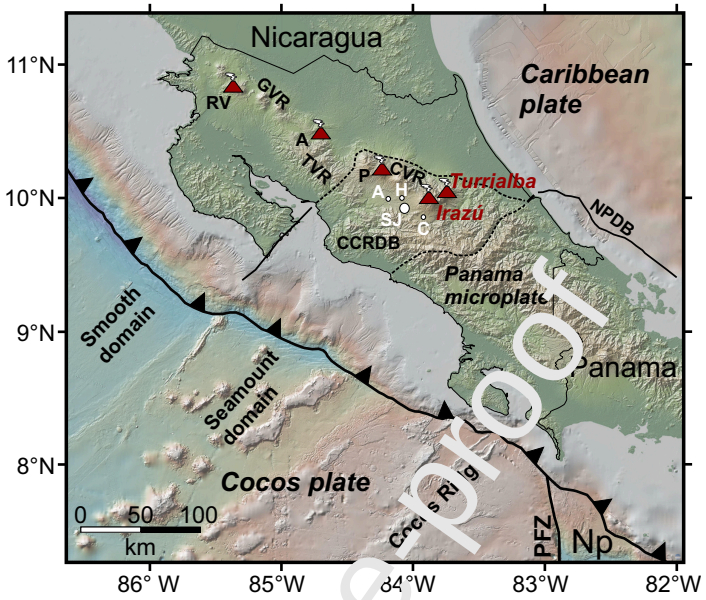

Figure 1: Simplified tectonic setting of Costa Rica and location of Turrialba volcano. Abbreviations are: Guanacaste volcanic range (GVR), Tilarán volcanic range (TVR), Central volcanic range (CVR), the Central Costa Rica Deformed Belt (CCRDB) and North Panama Deformed Belt (NPDB), Panama Fracture Zone (PFZ) and Nazca plate (Np) (Denyer et al., 2014). Black continuous and dashed lines represent faults. Triangles denote reverse faulting and point towards the overriding plate. Bathymetry and topography from Ryan et al. (2009). Active volcanoes are denoted by red triangles: Rincón de la Vieja (RV), Arenal (A), Poás (P). Main cities are indicated with white letters: SJ: San José, Alajuela (A), Heredia (H) and Cartago (C).

summit craters: the Southwest, which is the active one, the Central and the Northeast. They follow a NE-SW direction together with the pyroclastic cones Asnado and Tiendilla to SW and the avalanche amphitheater to NE, which is the result of an structural control by the Elia and Ariete faults which are part of the NE system (Soto, 1988; Linkimer, 2003; Calvo et al., 2019) (Figure 3). On the other hand, the NW fault system, contains the Río Sucio fault and the Liebres faults. The Río Sucio fault is presumed to be the source of a Ms 5.9 historical earthquake that occurred on December 30, 1952, 7 km NE from the crater of Irazú volcano, known as the Patillos earthquake (Montero and Alvarado, 1995). More recently, another important Mw 5.5 earthquake took place on December 1st, 2016 at 00:25 UTC, 7 km SE from the crater of Irazú volcano. This event, known as the Capellades earthquake, might have ruptured part of the Liebres fault (Linkimer et al., 2018) (Figure 2).

1.2. The 2010-present eruption

Tephrostratigraphic studies evidence at least 10 eruptions at Turrialba volcano during the last 7,000 years (Reagan et al., 2006; Alvarado et al., 2020). Since 1450 B.C. eruptions occurred with a period of around 230 years (Alvarado et al., 2020). The last and only known historical eruption, prior to recent activity, took place from September 1864 to February 1866, producing ash plumes that spread west, passing through most of the central valley and reaching the Pacific coast (Reagan et al., 2006; Alvarado et al., 2021).

The first signs of unrest related to the most recent eruption could possibly be traced back to the year 1982 when two seismic swarms occurred in the Irazú-Turrialba region (Güendel, 1984). Those were interpreted as tectonic by Alvarado et al. (1986), Barquero and Alvarado (1989) and Fernández et al. (1998). In 1987 there was still no sign of activity (Figure 4A). However during the second half of the 1990s Turrialba volcano showed physical, geochemical and geophysical signs of unrest (Tassi et al., 2004; Martini et al., 2010). The seismic activity increased slowly and progressively from several isolated swarms during the 1990s and early 2000s to a more abundant and varied seismicity since 2005 (Martini et al., 2010). The increase of volcanic activity became more visible in 2007 (Figure 4B), when the composition of fumarolic gases changed from a hydrothermal to a magmatic signature and seismicity increased

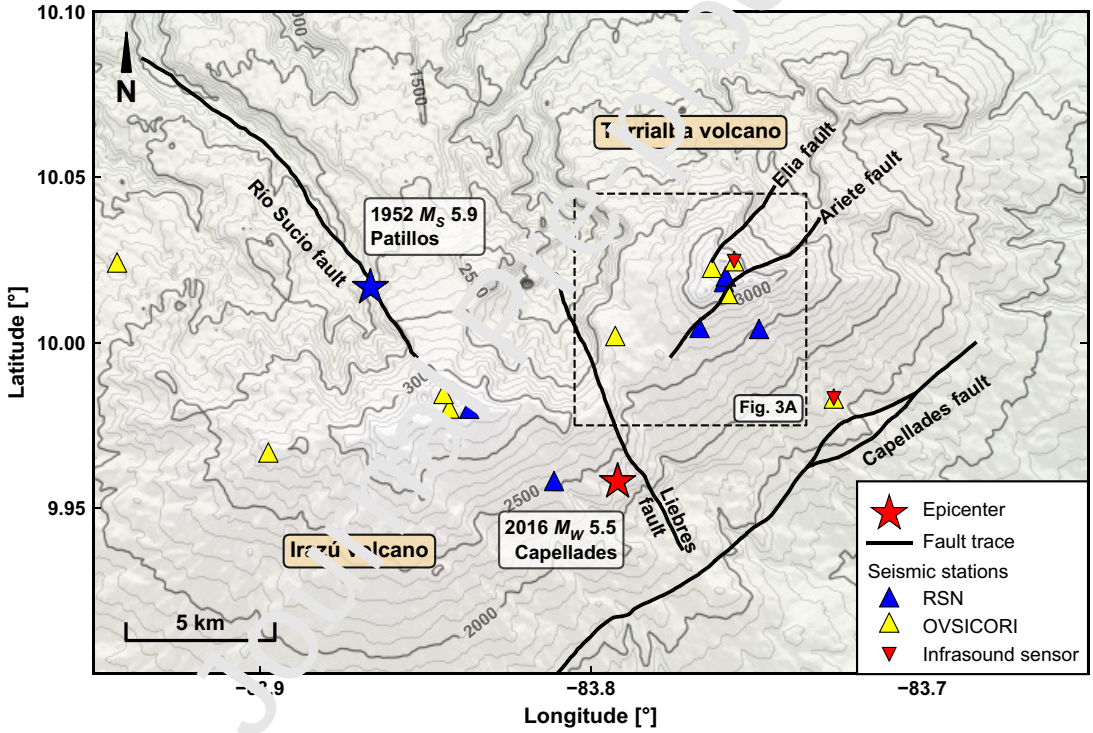

Figure 2: Irazú-Turrialba volcanic complex. Black lines are the main active faults Montero and Alvarado (1995); Montero et al. (2013); Linkimer et al. (2018). The 1952 Patillos earthquake 2016 Capellades earthquake (Mw 5.5) are shown with stars. The RSN and OVSICORI seismic stations are indicated with blue and yellow triangles, respectively. The rectangle indicate the zoom area showed in Figure 3. Topographic contour levels are shown every 100 and 500 m with thin and thick lines, respectively.

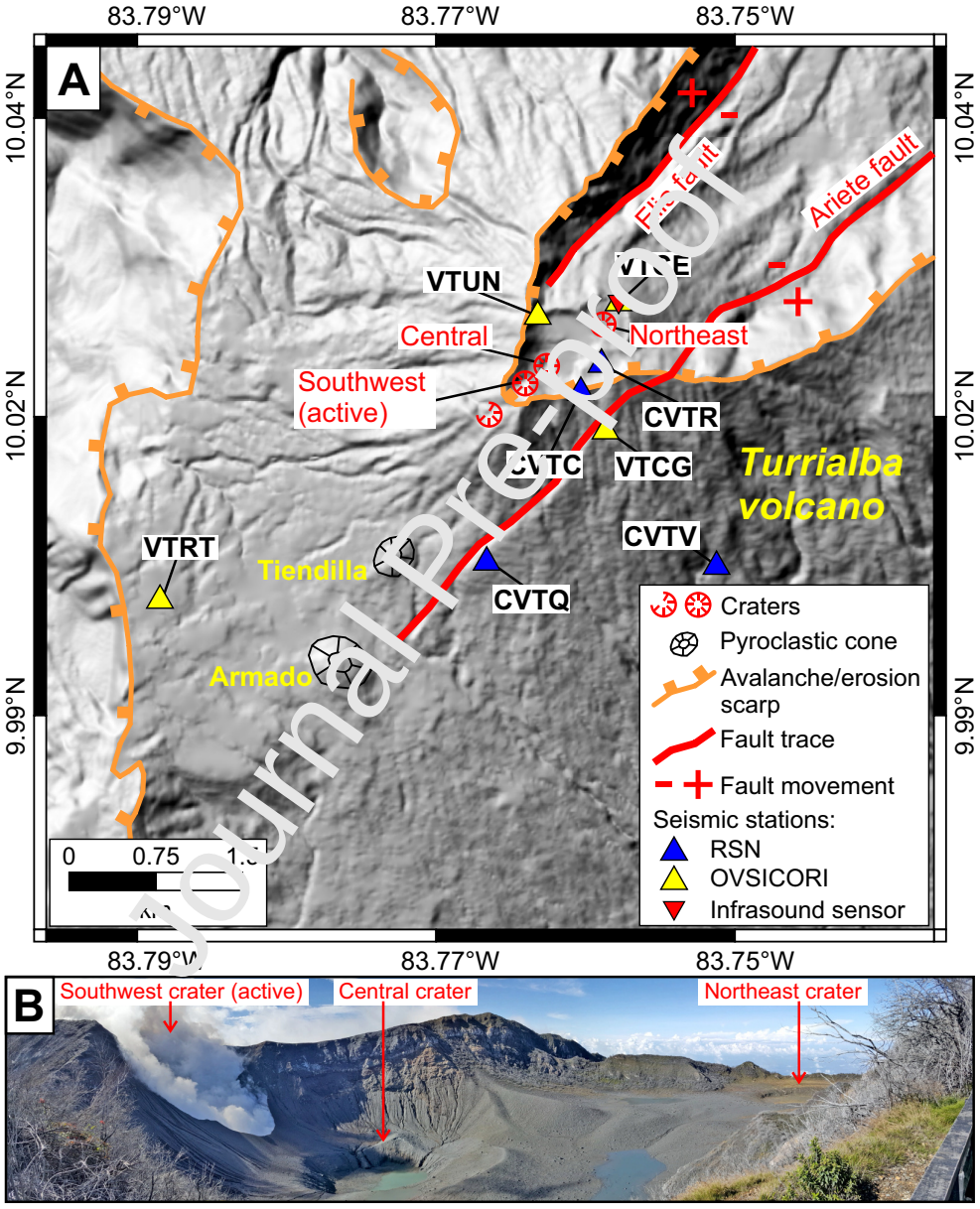

Figure 3: (A): Digital elevation model of Turrialba volcano with volcano-tectonic geomorphic features and seismic stations (triangles). Summit craters and Tiendilla and Armado pyroclastic cones, Elia and Ariete faults show a NE-SW trend. (B): Panoramic view of Turrialba volcano summit taken by Mauricio M. Mora on November 26, 2015, showing the Southwest (active), Central and Northeast craters.

(Hilton et al., 2010; Vaselli et al., 2010; Martini et al., 2010).

The first phreatomagmatic eruption occurred on January 5, 2010 (10:57 local time). It opened two vents in the SW inner wall of the active crater that became one on January 8, 2010 (Alvarado et al., 2016a), as it is observed in figures 4F and 5A. Minor ash emissions occurred on June, 12 and July, 13 later that same year (Soto and Mora, 2012).

On January 14, 2011, residents of a neighboring town (2.3 km from the active crater) informed about an ash fall and the presence of a strong smell of sulfur. However, no seismic activity was found that could indicate the occurrence of an explosion or volcanic eruption (Martínez and Pacheco, 2011). Later that year, on July, a new vent was observed on the W wall of the active crater. Another vent opened on January 12, 2012, on the SE external flank of the West crater. This event was accompanied by ash emission for a few hours. It was followed by a second ash emission from the same vent on January 18, 2012 (Figures 4F and 5C). On May 21, 2013 occurred a new ash emission that lasted 2 hours (Avard et al., 2012, 2013; Alvarado et al., 2016a). The ash came out simultaneously through the 2010 and 2012 vents (Figure 5D). For the 2012 and 2013 eruptions it was concluded based on geophysical and geochemichal records, that the events were caused by an excessive accumulation of gas at shallow depth (Avard et al., 2012, 2013).

On October 29, 2014, the volcano emitted ash for almost 13 hours in a sustained manner and ended with a 25-minute high-energy explosion that destroyed most of the eastern wall of the West Crater (Alvarado et al., 2016a) (Figures 4C and 5D, left). The explosion was followed by a practically continuous emission of ash that lasted about 3 days. The right image on Figure 5D shows the deposits scattered by the eruption towards the east. This eruption established a breaking point in the eruptive dynamics of Turrialba volcano, which shifted from annual isolated eruptive events to well-defined eruptive phases (Figure 5 right panel).

The first eruptive cycle lasted from October to December 2014, the second from March to June 2015 (an eruption on March 13, 2015 at 11:07 local time is shown in Figure 5E) and the third from October, 16 to October, 31, 2015. The last two cycles were separated by an eruptive episode on August 15, 2015. After the last cycle in 2015, some eruptions occurred between November and December 2015 in a context of low seismicity and expanded the area of the active crater as it is shown in Figure 4D. Subsequently, there were a few ash emissions and small isolated explosions between January and early April 2016.

A new eruptive stage began on 2016, with intense seismicity since April 27 and followed by a long-lasting ash emission on April 30. Finally, the explosive eruptive activity started on May 1, 2016 continuing until August 1 (Mora, 2016). After a short period of relative quiescence from August 1 until November 2016 a new explosive eruptive phase took place, with eruption columns reaching up to 4 km high (Mora and Soto, 2016). An example of this activity can be observed on Figure 5F.

On December 2016 a new open-vent eruptive phase started and waned on the first semester of 2019. It was characterized by frequent phreatomagmatic explosions, sustained ash emissions and Strombolian activity. Between July 2017 and May 2018 a lava pool was observed at the bottom of the active crater (Ruiz et al., 2017; Alvarado et al., 2020). The activity decreased during the first semester of 2019. A minor eruptive phase occurred between June and August 2020. Since then and until 2021 some infrequent eruptions have been observed, some of them explosive, that reached from 500 to 1000 m height. During this last eruptive period the active crater reached its current shape (Figure 4E and g). During 2021 infrequent phreatic explosions have occurred.

Based on the relative significance of each of the eruptive phases described above and their seismological characteristics that we will develop later, we selected four specific pre-eruptive stages (PES) to be analysed in more detail, in order to identify and characterize the precursory seismicity. The selected pre-eruptive stages will be referred from now on as PES and a roman number as follows:

- PES-I: from December, 2009 to January, 2010, which preceded the eruption of January 5, 2010.
- PES-II May, 2013, that preceded the May 21, 2013 eruption.
- PES-III from March to April, 2016, that preceded the open vent transition starting on April 30.
- PES-IV September, 2016, that preceded the definitive step towards an open vent system.

1.3. Previous seismological observations

Here we provide a brief overview of the seismological research conducted at Turrialba volcano. Mora et al. (2001) carried out a short campaign on March 12-14, 2001. They recorded 30 LP events with impulsive onsets and dominant

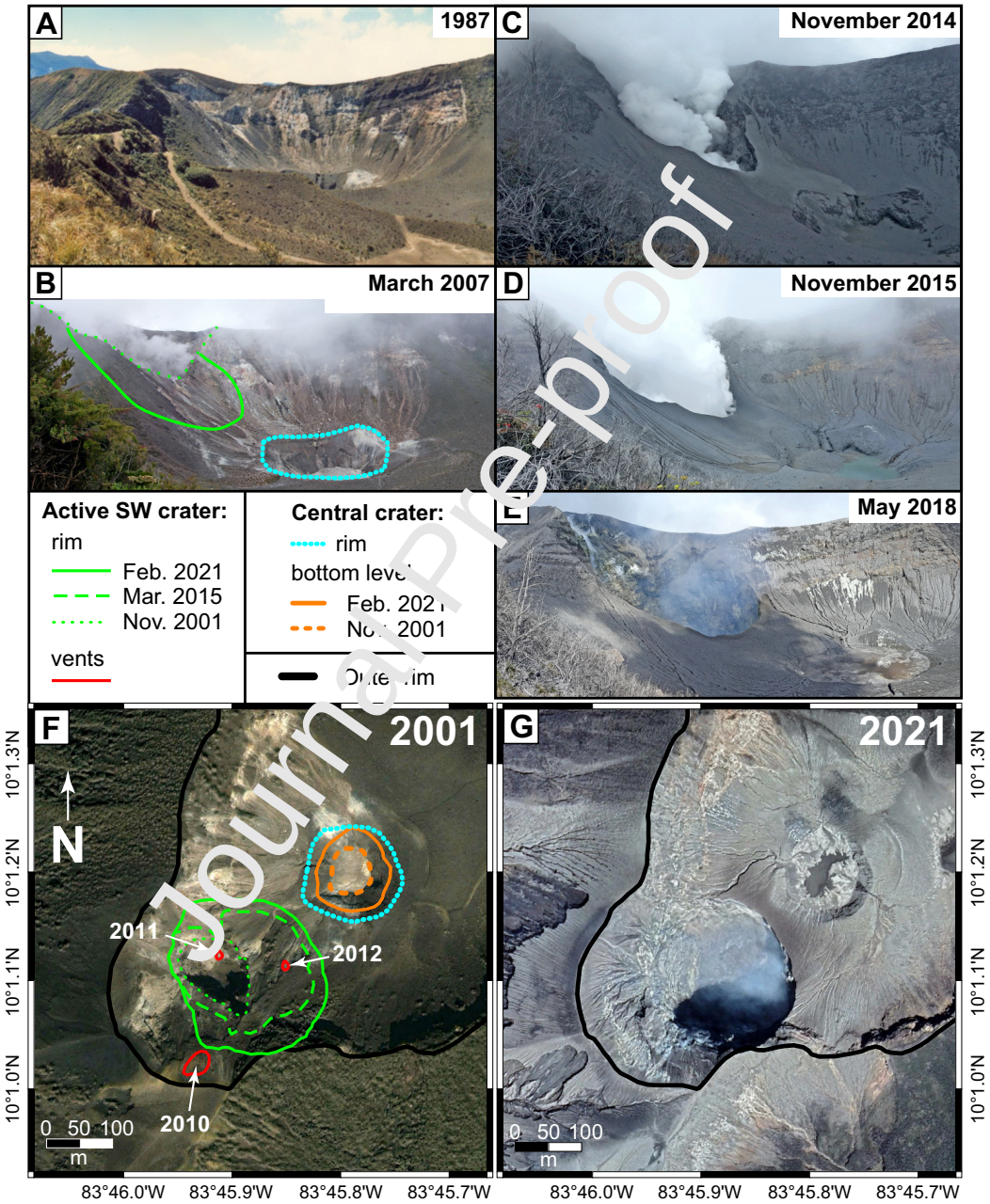

Figure 4: Temporal evolution of the active crater at Turrialba volcano from 1987 to 2021. (A-E): Photographs of the SW active crater and the central crater between 1987 and 2018. (F-G): Google Earth satellite images provided by Maxar Technologies and CNES/Airbus, respectively. The growing rim of the active crater is shown in (B) and (F). The progressive filling of the Central crater with pyroclastic material in indicated by the bottom level shown in (F). Photos in (A) and (B) are courtesy of Gerardo J. Soto. Photos from (C) to (E) were taken by Mauricio M. Mora.

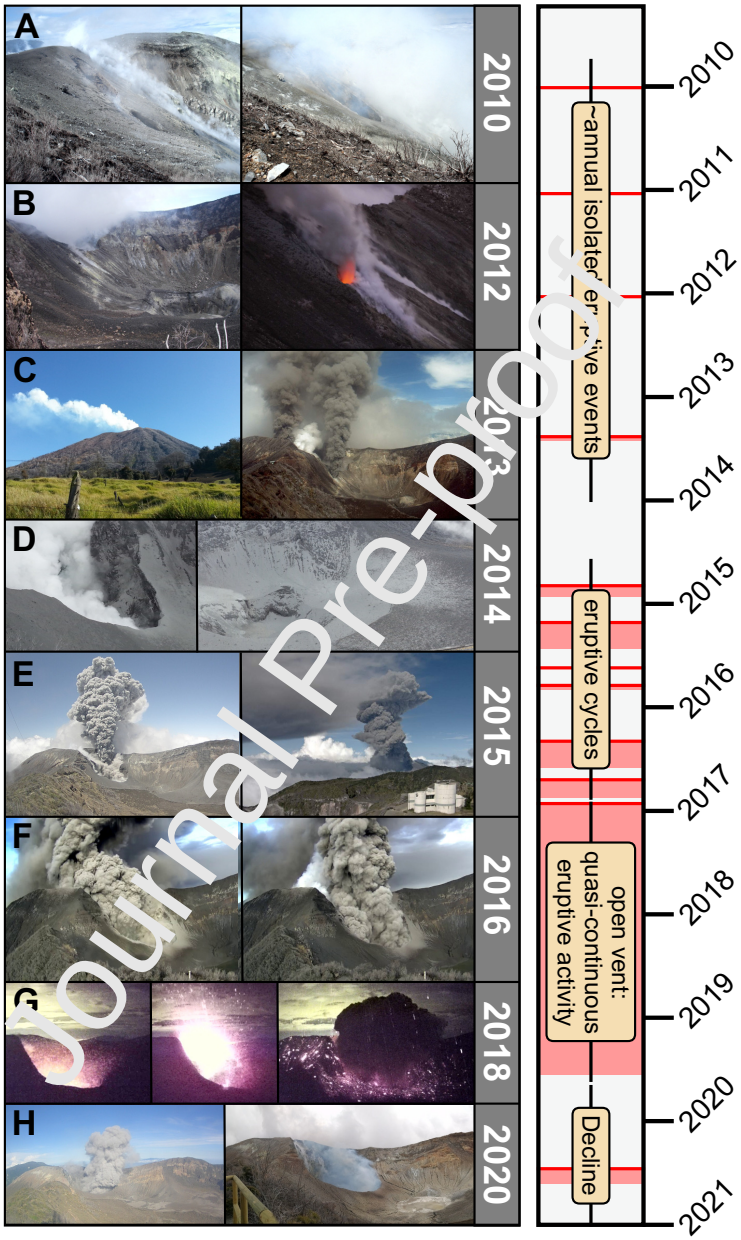

Figure 5: Left panel: Photograph examples of the activity. (A) Left, new vents formed by the eruption on January 4, 2010 and right: the vents joined. (Photographs by Mauricio M. Mora on April 13, 2011). (B) New vent formed in January 2012. (Left photo by Mauricio M. Mora and right by Javier F. Pacheco). (C) Left: Turrialba volcano degassing on January 31, 2013 (Photograph by Mauricio M. Mora) and right: eruption of May 21, 09:02 local time, taken by OVSICORI webcam. (D) Images obtained on November 1, 2014 after the explosion occurred on October 29, 2014. (Photographs by: Mauricio M. Mora). (E) Eruption on March 13, 2015 at 11:07 local time obtained by OVSICORI webcams at Turrialba (left) and Irazú (right) volcanoes. (F) Sequence of photographs from the RSN webcam, during an eruption on September 27, 2016 at 07:22 local time. (G) Sequence of photographs from the RSN webcam of an eruption on October 5, 2018 at 19:47 local time. (H) Left: Eruption on August 1 at 07:47 local time by OVSICORI webcam. Right: Image of the active crater degassing obtained on May 13, 2020 (Photo by Mauricio M. Mora). Right panel: Phases of the recent eruption (2010-2021) at Turrialba volcano. Solid red lines and pink areas show the start and span of each eruptive phase respectively.

frequency in the range 2-4 Hz, that were grouped in 3 families, denoting non destructive sources acting at that time. Tassi et al. (2004) provided a first classification and description of seismicity at Turrialba. They observed hybrid events with dominant frequency in the range 2.1-3.5 Hz and LP events with dominant frequency <1.8 Hz that were located 4-6 km beneath a 4 km elongated area comprising the summit craters and the northern flank. Martini et al. (2010) observed LP (0.8–1.8 Hz), tremor (2.4–3.1 Hz) and tornillo-type events. They also described two main VT swarms in April-May 2007 and September 2007.

A temporary installation of a broadband seismic network of 13 stations was carried out between March and September 2013 (Eyre et al., 2013). LP events recorded during that time period have been analysed in several papers. Eyre et al. (2013) and Zecevic et al. (2016) located those events through joint location-moment tensor inversion. They both found an elongated epicentral distribution oriented NE-SW at the summit located southeastward of the West and Central craters. Thun et al. (2015) observed step-like ground deformation near the summit in LP event recordings. Different models for the source mechanism of these events have been proposed. While Bean et al. (2014) suggested that LP events are caused by slow, quasi-brittle failure, Chouet and Dawson (2018) favored a fluid-driven crack model.

In 2018 Jiwani-Brown et al. (2020) installed 20 temporary broadband seismic stations around the Irazú-Turrialba volcanic complex. Their network was supplemented with 45 permanent stations from the regional networks (OVSICORI and RSN) and was utilized to produce an ambient noise tomography.

Since 2009 the RSN and OVSICORI observatories started to develop a network of broadband instruments at Turrialba volcano for monitoring purposes. In this paper we provide an overview of the seismological observations of the recordings of this network.

2. Data and methods

2.1. Seismic monitoring systems

The seismic surveillance at Turrialba volcano began in 1990, when the *Observatorio Vulcanológico y Sismológico de Costa Rica* (OVSICORI-UNA) installed a 1 Hz Ranger SS1 seismometer in the summit. In 1996, three short-period vertical L4C Mark Products seismometers were added. The first permanent broadband station, CIMA, was installed by RSN on September 2009, and it was equipped with a 30 s CMG-6TD. On September, 2011 it was replaced with a Guralp CMG-3T 120 s seismometer and the code changed to CVTR (Figure 3). This recording site became the RSN's reference station until the present. On the other side, OVSICORI set up VTUN as its reference station since April 2010 (Figure 3). It was equipped with a 120 s Nanometrics Trillium Compact and a Nanometrics Taurus recorder. In the following years, both observatories consolidated a broadband seismic network which is currently made up of more than a dozen stations (Figure 2). The seismic observations are complemented with visual monitoring from permanent webcams deployed by OVSICORI in 2010 and RSN since 2014 and infrasound instruments (Chaparral Physics 25 Vx) deployed in March, 2017 by OVSICORI.

2.2. Seismic events at Turrialba volcano

The seismicity at Turrialba volcano exhibit a wide variety of signals, the most significant ones can be described as follows (Figure 6):

- Volcano-tectonic (VT): typical high frequency events (1-30 Hz) generated by brittle fracture and movement along faults within the volcano. Those are divided in distal (dVT) and proximal (pVT), according to the distance to the active crater, and in shallow (<2 km) and deep (>2 km). dVT and deep events usually exhibit clear P and S phases, while pVT are shallow and have emergent onsets, non-detectable S phase and lower frequency (<5 Hz) contents than dVT.

- Long-period (LP): These signals have an emergent onset and a clear central pulse. The frequency content is generally restricted in a band between 0.5 and 4 Hz and the duration is of a few seconds (<5s).

- LP and tremor: This family is characterized by an LP event followed by a short tremor (a few minutes long). The tremor can have a broad-spectrum (1-20 Hz), hence it is called LP-T or a harmonic one (LP-HT) (van der Laat and Mora, 2017; van der Laat et al., 2018). The tremor may have also high-energy pulses (spasmodic character). The harmonic tremor coda exhibit a characteristic frequency gliding, very similar to the whooshes events observed at Arenal volcano (Benoit and McNutt, 1997; Mora, 2003; Lesage et al., 2006).

- Very long period (VLP): Pulses in the range from 2 and 100 seconds. A high frequency phase is usually superimposed.

- Tornillo (TOR): This is a variety of seismic-volcanic signals that are distinguished by a tonal or multitonal coda whose frequencies are stationary along the duration of the event and whose amplitude decays exponentially (van der Laat, 2020).

- Compounded tornillo (cTOR): They are characterized by an initial broad-spectrum event that often includes a VLP phase, followed by a multitonal coda typical of tornillo events (van der Laat, 2020). The frequency peaks of the coda are usually very numerous (up to 25) compared to typical tornillos. The first phase is impulsive and more energetic than the coda.

- Double phase (DP): These signals are characterized by an emergent first low-amplitude phase followed by a high amplitude one, variable duration, a characteristic frequency range of 2-12 Hz with peak frequencies between 5 and 9 Hz, and are followed by an acoustic phase (Pacheco, 2018). These events started in 2015 and often accompanied visually confirmed eruptive activity. For the most part, the associated eruptive activity were ash emissions (Figure S1), although some strombolian explosions were accompanied by a similar two-phase signal (Figure S2). Pacheco (2018) found very low values of volcano acoustic-seismic ratio (VASR) indicating a greater seismic than acoustic coupling of the explosions.

- Drumbeats (DB): Repetitive LP events with characteristic frequencies between 2-14 Hz and inter-event intervals in the range of 6 - 10s. Sequences of drumbeat events were observed in 2010, 2012, 2013, 2017 and 2018. Lesage et al. (2018) analyzed the sequence recorded in 2017. According to them, the clearest episode occurred on 27 January, 2017 from 03:00 to 05:45 UTC and it was composed of about 600 small earthquakes with remarkably similar waveforms but with varying amplitudes.

- Tremor: It is a ground vibration that lasts tens of minutes to several hours. Its spectrum can be broad band (1-5 Hz) and non-harmonic (T) or more narrow-band and be harmonic, with one and sometimes two sets of evenly spaced dominant peaks. Mora and Pacheco (2018) and Mora et al. (2019) performed a detailed spectral analysis from a catalog of 2044 episodes of harmonic tremor that covers the period between 2009 and 2019. In the long-term, they observed a progressive increase in the number of episodes of harmonic tremor with time as well as significant variations in the fundamental frequency (range of 0.4 and 3.5 Hz) and in the number of overtones.

2.3. Analysis of continuous recordings

For the long-term analysis we use the real-time seismic energy measurement (RSEM) (De la Cruz-Reyna and Reyes-Dávila, 2001) computed from seismic records obtained at CVTR (previously CIMA) and complemented with those obtained at VTUN to fill the gaps (~5%). Records were first corrected for instrument response and then band pass filtered between 1 and 24 Hz. The RSEM was calculated using 1-minute segments. The results were decimated by taking the daily median value. Finally, the data were displayed using a 5-day moving median. To correct the RSEM amplitudes due to different stations used, a correction factor was obtained to compensate for site and trajectory differences.

We complemented the seismic observations with SO_2 measurements obtained by Conde et al. (2014) and further completed by OVSICORI-UNA using a scanning dual-beam Mini-DOAS (Conde et al., 2014). We also used petrographic ash analysis measurements obtained from OVSICORI databases (Supplementary Figure S12), partially published in Alvarado et al. (2016a).

2.4. Analysis of discrete events

In order to seek for significant precursory events of the eruptive phases, a close inspection of the time domain records and detailed time-frequency analysis were carried out. We also used the REDpy algorithm (Hotovec-Ellis and Jeffries, 2016) to group the events and obtain specific catalogs.

We focused on TOR, LP-HT, DP, HT and VT events since each of those types of signals carries significant information about the volcanic system. We implemented specific analysis for each type to better constrain their characteristics:

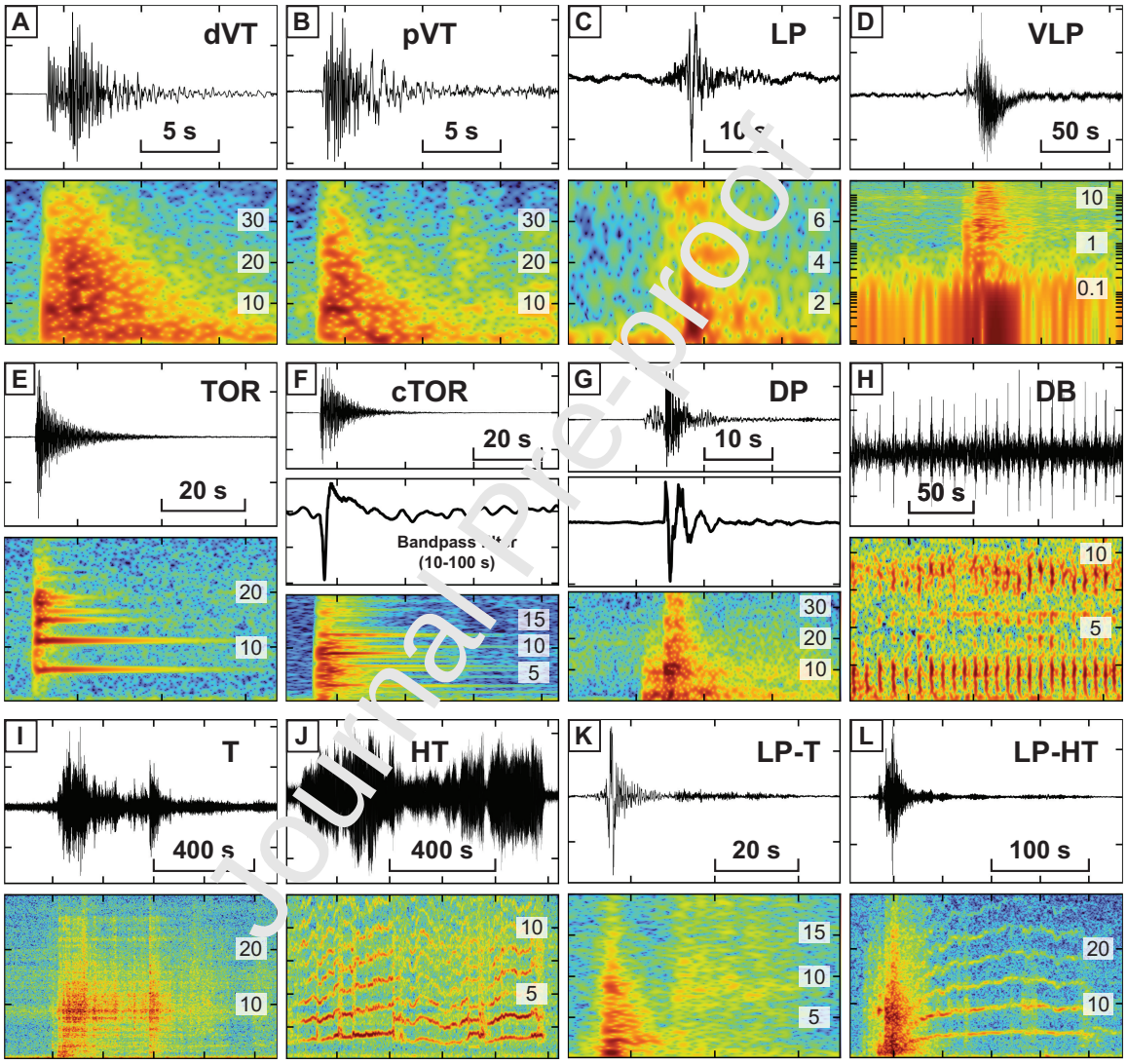

Figure 6: Typical seismicity of Turrialba volcano. For each type of event the velocity trace (above) and the corresponding spectrogram (below) is depicted. For the cTOR event in (F) an additional bandpass-filtered trace (middle) is provided. For the double phase event (DP) both seismic (above) and infrasound (middle) traces are shown in (G). All events, except the DP event, were recorded by RSN's CVTR station. The DP's seismic and infrasonic records come from OVSICORI's VTCE station. Abbreviations are as follows: dVT: distal volcano-tectonic, pVT: proximal volcano-tectonic, LP: long period, DB: drumbeat; VLP: very long period, DP: double phase; TOR: tornillo; cTOR: long period event with tonal coda; T: tremor; HT: harmonic tremor; LP-T: long period event with tremor; LP-HT: long period event with harmonic tremor.

- TOR and cTOR events analysis: As these signals share a multitonal coda with stationary non-regularly spaced spectral peaks, we analyzed each peak independently. For each event, the signal was first bandpass filtered in the 1-30 Hz range. To extract the peaks from the Fourier spectrum, a threshold was obtained by smoothing the spectrum with a Savitzky-Golay filter (Savitzky and Golay, 1964) of order 1 and a 3 Hz window. Only the peaks whose amplitude exceeded twice the corresponding value in the smoothed spectrum were extracted. In addition, the search for peaks was restricted to a minimum distance of 0.3 Hz between peaks and a minimum amplitude of 0.04 (value normalized by the maximum amplitude).

- Location of VLP phases of cTOR events: Because very low frequency waves are not affected by site effects, particle motion analysis was used to locate the VLP phase of cTOR events (Caudron et al., 2018). The signal was first bandpass filtered between 8 s and 16 s and then we used a 20 s window around the pulse. The azimuth and angle of incidence of wave propagation were obtained from the orthogonal regression adjustment of the movement in the horizontal plane and in the radial vertical plane using the algorithm implemented in the ObsPy package (Beyreuther et al., 2010). The final solution was retrieved from the intersection of the propagation vectors obtained at several stations. The mean square error in each dimension is reported.

- DP events analysis: We also carried out an specific overview of these events in order to determine which were associated with eruptive activity. We used the images from the permanent webcams. The events were classified in three types: 1) uncertain, due to adverse atmospheric conditions or the presence of a constant gas and/or ash plume from the active crater; 2) not eruptive; and 3) eruptive. Types 2 and 3 are certain because clear images were available.

- LP-HT events: A semi-automatic processing based on the cepstrum (Noll, 1967) was implemented to seek for the fundamental frequency f_1 of the harmonic tremor associated to these events. f_1 corresponds to the dominant cepstrum quefrency. The analysis is performed in a moving window of 5 s with a step of 1 s. For each event we recorded the initial, final, minimum, maximum, average and standard deviation of f_1. In addition, the number of harmonic overtones were manually counted.

- Harmonic tremor: We first built a catalog with the extracted traces by manual inspection. We used the spectrogram to obtain the fundamental frequency f_1 at each window in order to account for the gliding. We then obtained the average, median and mode of the fundamental frequency, and the number of overtones.

- VT seismicity was obtained from a joint catalogue compiled from OVSICORI and RSN data from 2010 onwards. For this period the locations are good enough to be analyzed. From 2010 backwards we do not have good station coverage as the seismic monitoring systems at Irazú and Turrialba were incipient as we mentioned in subsection 2.1. The VT catalogue comprise the locations, depth, magnitude (Ml) and uncertainties coming from routine processing. The velocity model used for the location comes from Quintero and Kissling (2001) and was modified to include a layer between 0 and 4 km of elevation above sea level with a P and S-wave velocities of 3.2 km/s and km/s, respectively.

3. Results

This research was developed using two time scales. We first analyzed the seismicity in a long-term basis to characterize the evolution of the activity between 2009 and 2020 (Section 3.1). Secondly, we carried out a detailed analysis focusing on the precursory seismicity of the main eruptive stages (Section 3.2).

3.1. Long-term analysis

3.1.1. RSEM and pre-eruptive tremor abatement (PETA)

To obtain a long-term overview of the seismic activity at Turrialba volcano we used the RSEM (Section 2.3) and compared it with the SO_2 measurements (Figure 7). In general, the highest RSEM values occurred prior and immediately after the first eruption on January 2010 and during the period between May 2016-May 2017. In between those periods (years 2011-2015) the RSEM remained in lower levels. After May 2017 the RSEM decreased gradually.

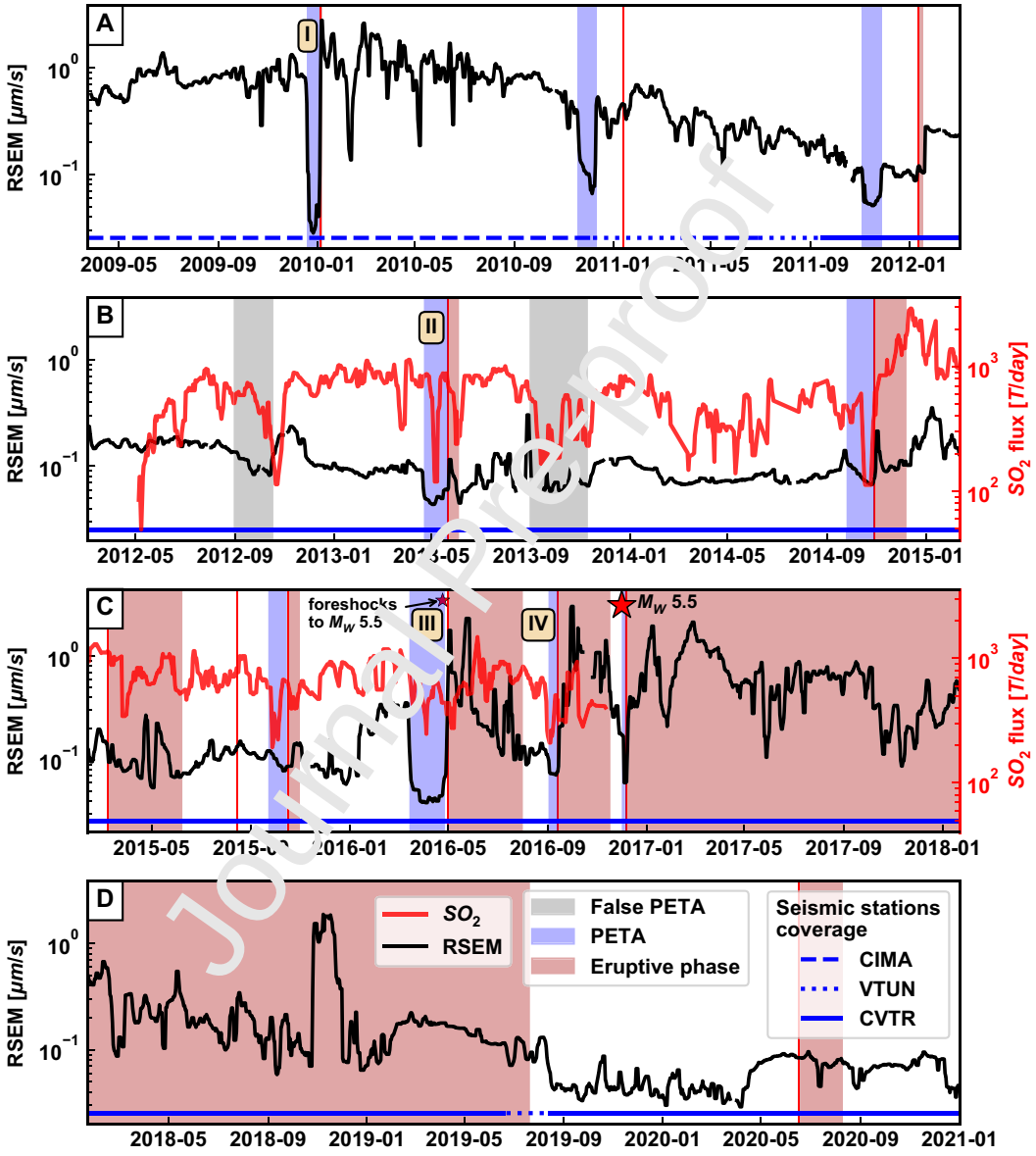

Figure 7: RSEM and SO_2 flux between 2009 and 2020. Vertical red lines and bands indicate the eruptive phases onset and time-span, respectively. Vertical blue bands indicate pre-eruptive tremor abatement (PETA). Vertical gray bands indicate periods of tremor and SO2 flux abatement that do not precede an eruptive event or phase. The horizontal line in the lower part of the plot indicates the station used for the RSEM computation as in the legend. The roman numbered labels indicate the pre-eruptive stages (PES) analysed in detail in this work. The Mw 5.5 Capellades earthquake and its April foreshock swarm are indicated by a large and a small red star, respectively.

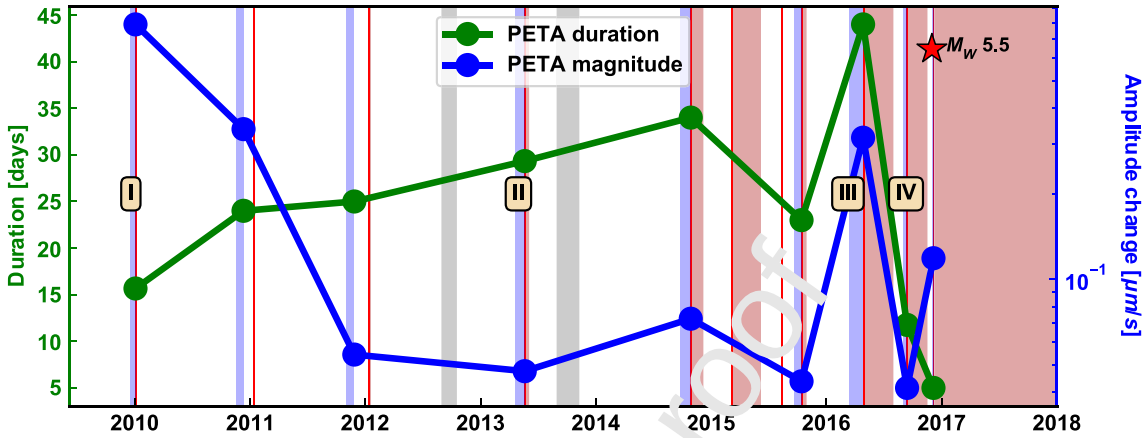

Figure 8: Evolution of the characteristics of the PETA periods. The abatement magnitude was computed as the difference between the maximum RSEM amplitude during the 7 days prior the PETA period and minimum amplitude during the PETA period. The Mw 5.5 Capellades earthquake is indicated by a red star. Roman number labels, vertical red dot lines and gray bands are the same as in Figure 7.

A relevant precursory feature identified in this analysis is a decrease in the seismic energy prior to most of the eruptive phases. For clarity, we will refer to this feature as a *pre-eruptive tremor abatement*, hereinafter abbreviated as PETA. Each PETA period is indicated with a vertical blue band in Figure 7 and following time series representations. This behaviour was observed in 9 occasions being more conspicuous for the January, 2010 and April, 2016 eruptive phases. In general, we observe a decrease in the abatement magnitude, i.e. the amplitude difference between the maximum RSEM amplitude during the 7 days prior the PETA period and the minimum amplitude during the PETA period (Figure 8). On the contrary, the duration of the PETA increased up until the April, 2016 period, and drastically dropped later that year (Figure 8).

In some PETA period cases the decrease was drastic and the low amplitudes were sustained prior to the eruptive phase onset (*inverse plateau*), while in others, the decrease in amplitude was progressive and constant (Figure S3 in Supplementary Material). Two of the PETA periods identified occurred with a considerable temporal separation (~1 month) before the corresponding eruptions in early 2011 and early 2012 Figure 7A.

Since a correlation between the seismic activity and the magmatic gas flux has been established in other studies (Conde et al., 2014; Chaussidon et al., 2017) we broadly compare the RSEM to the SO_2 flux (in red in Figure 7). For example, for the 2014 eruptive phase, de Moor et al. (2016) reported the concomitant decrease of SO_2 flux and seismic amplitude. In this work, we observe this behavior in all PETA periods occurring during the period with available data.

Furthermore, we observe two other periods when RSEM and SO_2 decrease, in September, 2012 and September, 2013, but that were not followed by an eruption. These periods are indicated by the vertical gray bands Figure 7. Although, by the end of these periods no eruptive activity took place, some interesting seismic activity is noted. For the September, 2012 period, the RSEM increase was associated with a drumbeat sequence of LP events (Figure S4 in Supplementary Material). For the September, 2013 period, a sharp increase of TOR events was observed (Figure 10).

3.1.2. Volcano-tectonic seismicity

The VT seismicity beneath the Irazú-Turrialba volcanic complex was distributed in two zones: 1) a broad (~12 km) zone beneath the Irazú edifice between 0 and 4 km below sea level (dVT); and 2) a tighter cluster at Turrialba volcano between 0 and 3 km above sea level (pVT, Figure 9). Additionally, we observe that from 2015 to 2017 the VT seismicity progressively moved from Irazú (dVT) to Turrialba volcano (pVT) (Figure S5 in Supplementary Material).

The temporal distribution shows two periods of major activity. The first occurred from 2012 to 2014 with a sharp increase in October, 2012, after the Mw 7.6 Nicoya earthquake (September 5, 2012) (Lupi et al., 2014). The second occurred from mid 2014 to 2017. During this period occurred the Capellades seismic sequence (main shock depicted as a red star in figures 2 and 9), the climax of volcano-tectonic seismicity between 2009 and 2021 (Figure 9C and D).

This sequence started with some foreshocks on April 24, 2016 (Linkimer et al., 2018), during a PETA prior to the May 2016 eruptive cycle.

We used the relationship between the cumulative seismic moment of the VT events and the geodetic estimation of the intruded magma volume found by White and McCausland (2016). Based on the VT seismicity, we estimated a volume equal to 0.016 km^3. This result is consistent with the estimation based on geodetic data carried out by Müller (2018) who modeled a magma reservoir beneath the Irazú volcano at 8 km depth where an intrusion of 16 Mm^3/year occurred during 2015 and 2016 (Battaglia et al., 2019). If we accumulate this rate of intrusion in the course of two years, it yields a total volume change of 0.032 km^3, which is in the same order of magnitude of our results. Furthermore, this match is in the variability range of the data collected by White and McCausland (2016) and Meyer et al. (2021) (Figure S6 in Supplementary Material). As those authors explain, the cumulative seismic moment is dominated by the few larger events. Thus, the Capellades earthquake must be related to the magma intrusion in order to account for the geodetic estimation by Müller (2018).

3.1.3. Long-term evolution of discrete TOR, DP and HT events

TOR events were first observed in 2012 and their number had a significant increase during the second half of 2013, after the May eruption (Figure 10A). This was coincident with the RSEM and SO_2 decrease period that occurred in September 2013 (gray vertical band in Figure 10). In the following 2014 and 2015 years the number of events decreased, although an important increase was observed in October 2015 (Figure 10A). Between 2012 and 2013, the frequency of the first spectral peak decreased from 10 to 2 Hz (Figure 10B). Then, in 2014 this frequency went up suddenly up to 12-18 Hz. Finally during 2015 it diminished again down to 2 Hz. In 2016 cTOR became dominant showing lower frequencies down to 0.6 Hz by September 2016. Preliminary estimations of the coda attenuation quality factor of representative TOR and cTOR events (Lesage, 2008, 2009) indicate that TOR events could have beeen related to the resonance of a suspension of ash in gas (Q ~600), while cTOR events could have been related to bubbly water or bubbly basalt (Q ~60-80), following Kumagai and Chouet (2000) (Supplementary Tables S1 and S2).

DP events started in 2015 (Pacheco, 2018) and reached a maximum number in November 2015 (Figure 10C). Afterwards, a progressive but fluctuating decrease in the number of events can be observed (Figure 10C). Several DP events accompanied eruptions, becoming more usual since 2017 (Figure 10C).

Harmonic tremor (HT) has been observed in Turrialba volcano since 2007 (Martini et al., 2010). However, our catalog extends from 2009 to 2018. Between 2009 and 2013 HT episodes were rare, but as of 2014 they became more conspicuous, particularly in 2018 when they reached a maximum (Figure 10D). In parallel, the number of overtones also showed a slight increase (Figure 10F). The fundamental frequency (f_1), however, fluctuated between 0.5 to 3 Hz. The lowest frequencies were reached during 2015 (Figure 10E).

3.2. Short-term analysis of the studied pre-eruptive stages (PES)

In section 1.2 we defined 4 pre-eruptive stages to be studied in detail from the seismological point of view. Each PES was dominated by a different type of seismic-volcanic event, but some families were present in several stages (Table 1). LP-HT events were observed in PES I-III, but mostly in PES-I. LP-T events were only observed in PES-II. The cTOR events were observed mainly in PES-III and PES-IV. Finally, DP events were only recorded on PES-III and PES-IV. We highlight that the most important family in number is the LP-HT, which has the highest average rate and is present in all stages. Also, in all of the stages a swarm of pVT events was observed towards the end of the stage.

Table 1: Average rate (events per day) of type of event at each pre-eruptive stage

PES	Start date	End date	Duration [days]	LP-HT	LP-T	TOR/cTOR	DP
PES-I	2009-12-19	2010-01-03	16	66	0	0	0
PES-II	2013-04-21	2013-05-21	29	3	42	0.2	0
PES-III	2016-03-14	2016-04-27	44	9	0	21	0.6
PES-IV	2016-09-02	2016-09-12	11	0	0	4	0.6

LP-HT events were more frequent during the PES-I. In this 16-day period a total of 1054 events occurred, with a maximum rate of 8 events per hour. On the other hand, PES-II and III were longer (29 and 44 days, respectively), but presented fewer LP-HT events (71 and 429, respectively). No LP-HT were detected on PES-IV. We statistically compared their characteristics per PES (Figure 11). The amplitude and the mean fundamental frequency (Mean f_1)

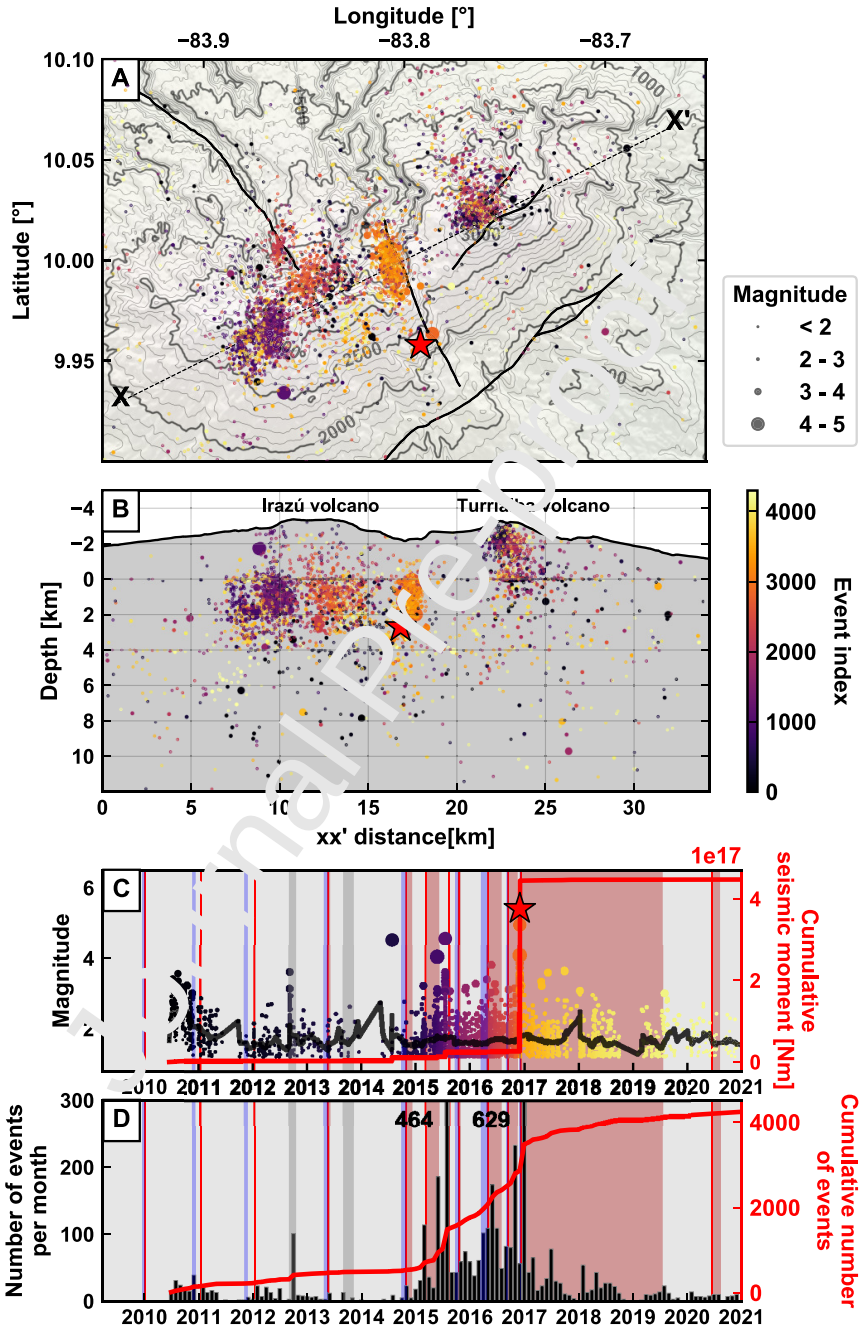

Figure 9: Volcano-tectonic (VT) seismicity in the Irazú and Turrialba volcanic complex. (A): Map: Black lines are the main active faults Montero and Alvarado (1995); Montero et al. (2013); Linkimer et al. (2018). The XX' dashed line indicates the trend of the profile in (B); (B): XX' profile; (C): magnitude time series and cumulative seismic moment of VT events; (D): Number of VT events per month, the number of events in August 2015 and December 2016 is indicated next to each bar, in order to provide a vertical scale adjusted to the minor variations. The color of each point is dependent on the order of occurrence as shown in the colorbar. The red star in (A) to (C) indicates the Mw 5.5 Capellades main shock. The Liebres fault is indicated with a dashed line in (A) and (C). Color coding for vertical lines and bands as in Figure 7. We use a minimum magnitude cut-off of 1.2 based on the analysis of the Gutemberg-Richter Law.

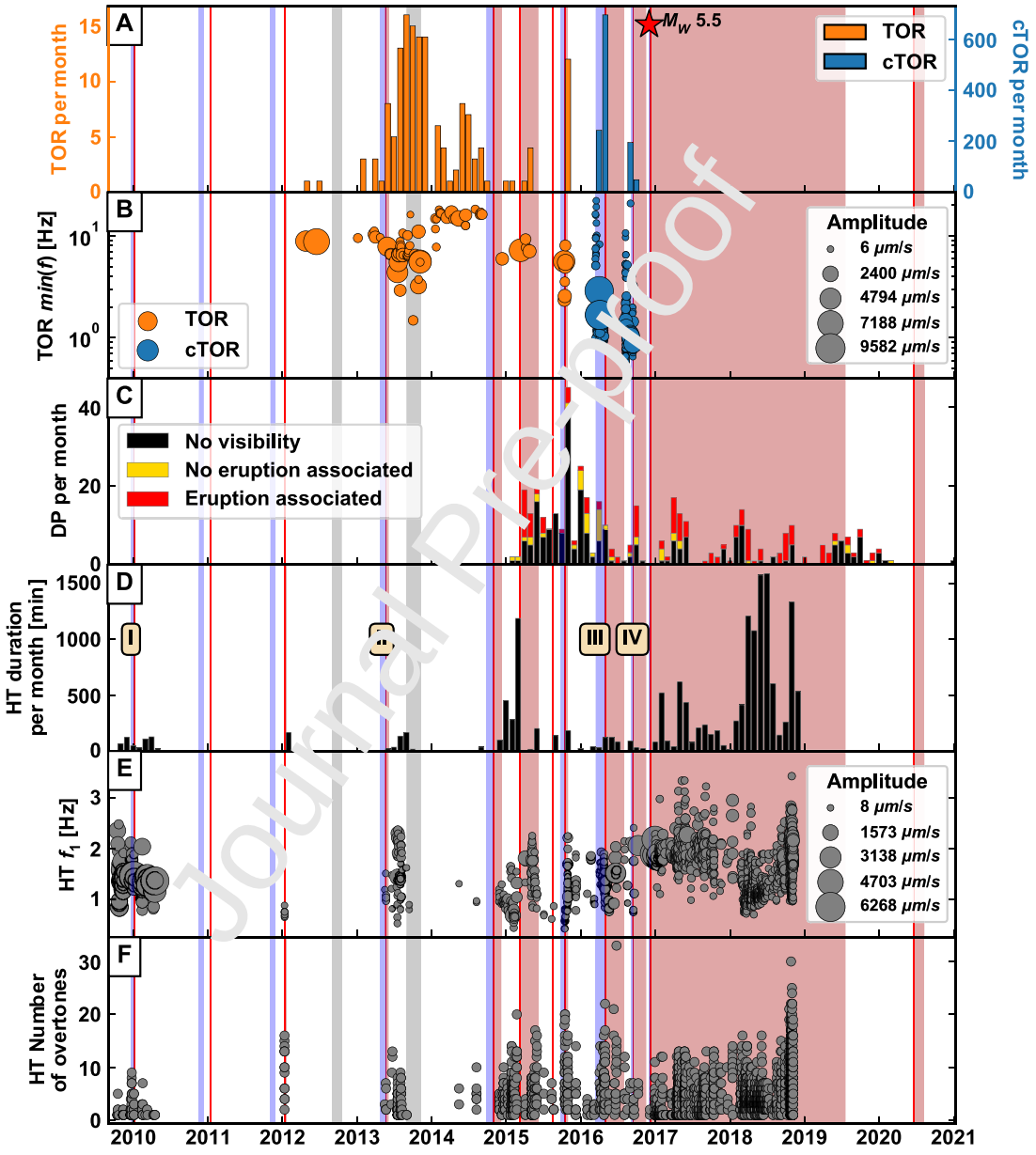

Figure 10: Evolution of the tornillo-type (TOR), double-phase (DP) and harmonic tremor (HT) events. (A): Number of TOR and cTOR events per month. (B): Frequency of the first spectral peak of TOR and cTOR events. (C): Number of DP events per month. (D): HT duration per month. (E): HT fundamental frequency (f_1). (F); HT number of harmonic overtones. Roman number labels, vertical red dot lines and color bands are the same as in Figure 7. The Mw 5.5 Capellades earthquake is indicated by a red star.

showed a progressive decrease along each PES, while the number of harmonic overtones remained the same for PES-I and II, but increased in PES-III. In two instances of LP-HT events we observe intermittence of the odd harmonics (Supplementary Figure S13) which can be understood as period doubling (Julian, 1994; Rust et al., 2008; Hagerty et al., 2000).

LP-T events occurred only during PES-II. LP-TH and LP-T share some similarities on the LP part, with a dominant frequency of 1.5 Hz and typical duration of 20 s. Remarkably, LP-HT occurred in the second half of the PES, when the RSEM started to increase prior to the May 21, 2013 eruption (Figure S7 in Supplementary Material).

cTOR events were important precursors during PES-III and IV, when 943 and 245 events occurred, respectively. For PES-III, cTOR events were grouped by cross-correlation, using the REDPy algorithm (Hotovec-Ellis and Jeffries, 2016). We first filtered the signals using a Butterworth bandpass filter between 1-10 Hz and order 4. Then, we set minimum correlation coefficient of 0.7 to group the events. From the 943 manually detected events, 72% (678 events) were grouped into 66 families. Of the grouped events, 537 events (80%) belong to six families made up of more than 14 events each. Using a stacked waveform per cluster, the particle motion analysis yields towards a consistent source location beneath the central crater ~500 m deep (Figure S8 in Supplementary material).

We also extracted each spectral peak for the cTOR events for a detail time-frequency analysis (Figure 12). In contrast to the typical proportional shifting of all spectral peaks (gliding) of the HT spectral peaks, we can observe that those of cTOR and TOR events varied independently. Due to the narrow frequency range of variation of the spectral peaks (<1 Hz), the scale in Figure 12 was adjusted for each peak. The same data is displayed in a common frequency and amplitude scale in Supplementary Figure S9 for direct comparison between peaks. During PES-III, a general pattern of frequency variation can be established: a prolonged decline followed by two cycles of rise and fall.

Mora and Alvarado (2016) reported three VT swarms that occurred on April 15, April 24, and April 26 2016, repectively (vertical blue lines in Figure 12). These were concomitant with each minimum frequency of the cTOR peaks. For each VT swarm, RSN located at least 1 event. Although, the rest of the events were not located due to a poor signal-to-noise ratio (SNR) and/or network coverage, the catalog was completed using the REDPy routine (van der Laat and Linkimer, 2019) (Figure S10 in Supplementary material). The April 15 dVT swarm was located in the north flank of Turrialba volcano. The April 24 dVT swarm, was located between Irazú and Turrialba volcanoes and it is a foreshock swarm of the Mw 5.5 Cinchillades (Linkimer et al., 2018). Finally, the April 26 pVT swarm, was located near the active crater of Turrialba volcano at shallow depths (<1 km).

During PES-IV, the frequency of cTOR spectral peaks continued to decrease (>0.75 Hz), especially during the last 24h before the September 13, 2016 eruption onset (Figure S11 in Supplementary material).

4. Discussion

4.1. Interpretation of the pre-eruptive tremor abatement (PETA) periods

Although not termed PETA, similar behaviour (i.e. a decrease in seismic amplitude previous to eruptive activity) has been reported in other volcanoes and in a variety of time-scales. For example, at Redoubt volcano, a short-lived (seconds to minutes) seismic pause was observed prior to some Vulcanian explosions following gliding harmonic tremor (Dmitrieva et al., 2013; Hotovec et al., 2013). Similarly, at the Suwanosejima volcano, some Vulcanian explosions have been preceded by a sudden cessation of tremor on a short-term scale (minutes) (Nishimura et al., 2013). In Telica volcano, Roman et al. (2016) showed that episodes of seismic inactivity on a medium-term scale (minutes to hours) systematically preceded the explosions in May 2011. In the same volcano, Geirsson et al. (2014) and Rodgers et al. (2015) reported a decrease in tremor amplitude and in the number of discrete seismo-volcanic events over a long-term period (weeks), between March and April prior to the May 2011 eruption. This last example is similar to Turrialba volcano, in which the PETA periods last for several days to over a month.

In other volcanoes this tremor quiescence has been interpreted as a pause in the circulation of fluids and/or ash in the shallow part of the volcanic edifice due to the sealing or blockage in the conduits. The resulting overpressure would eventually provoke rock failure and, consequently, the eruptive activity (Nishimura et al., 2013; Geirsson et al., 2014; Rodgers et al., 2015; Roman et al., 2016). Particularly, for Turrialba volcano, the concomitant decrease in SO_2 flux with PETA periods suggests the blockage in the system. The cause of this sealing can be related to the precipitation of minerals from rising magmatic gases (de Moor et al., 2016; Stix and de Moor, 2018). For Turrialba volcano, this hypothesis is supported by the collection of blocks of highly indurated hydrothermal breccia that were

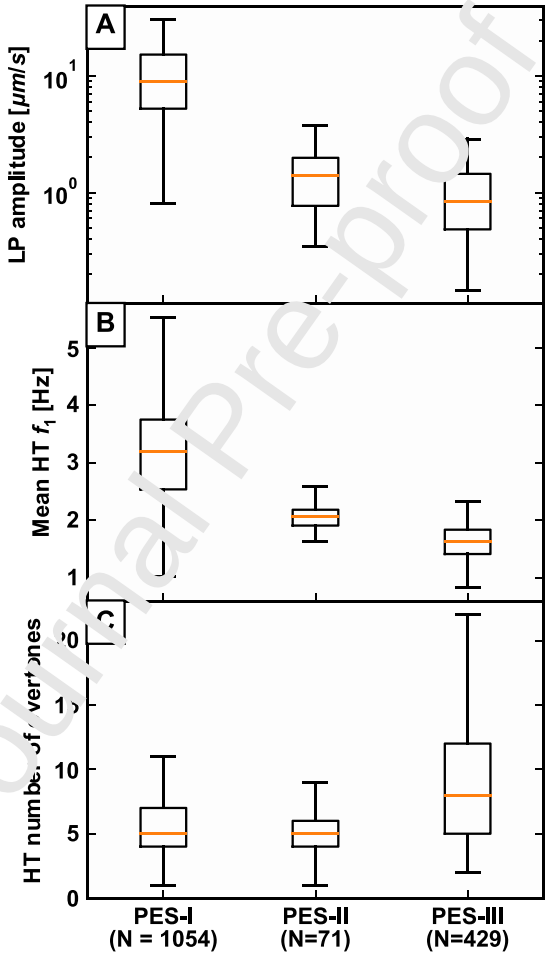

Figure 11: LP-HT events characteristics at each pre-eruptive stage (PES). (A) Amplitude of the LP event part; (B): mean fundamental frequency f_1 of the harmonic part; (C): number of overtones of the harmonic tremor part. In each case, the box extends from the lower to upper quartile values of the data, with an orange line at the median. The whiskers extend from the box to show the range of the data.

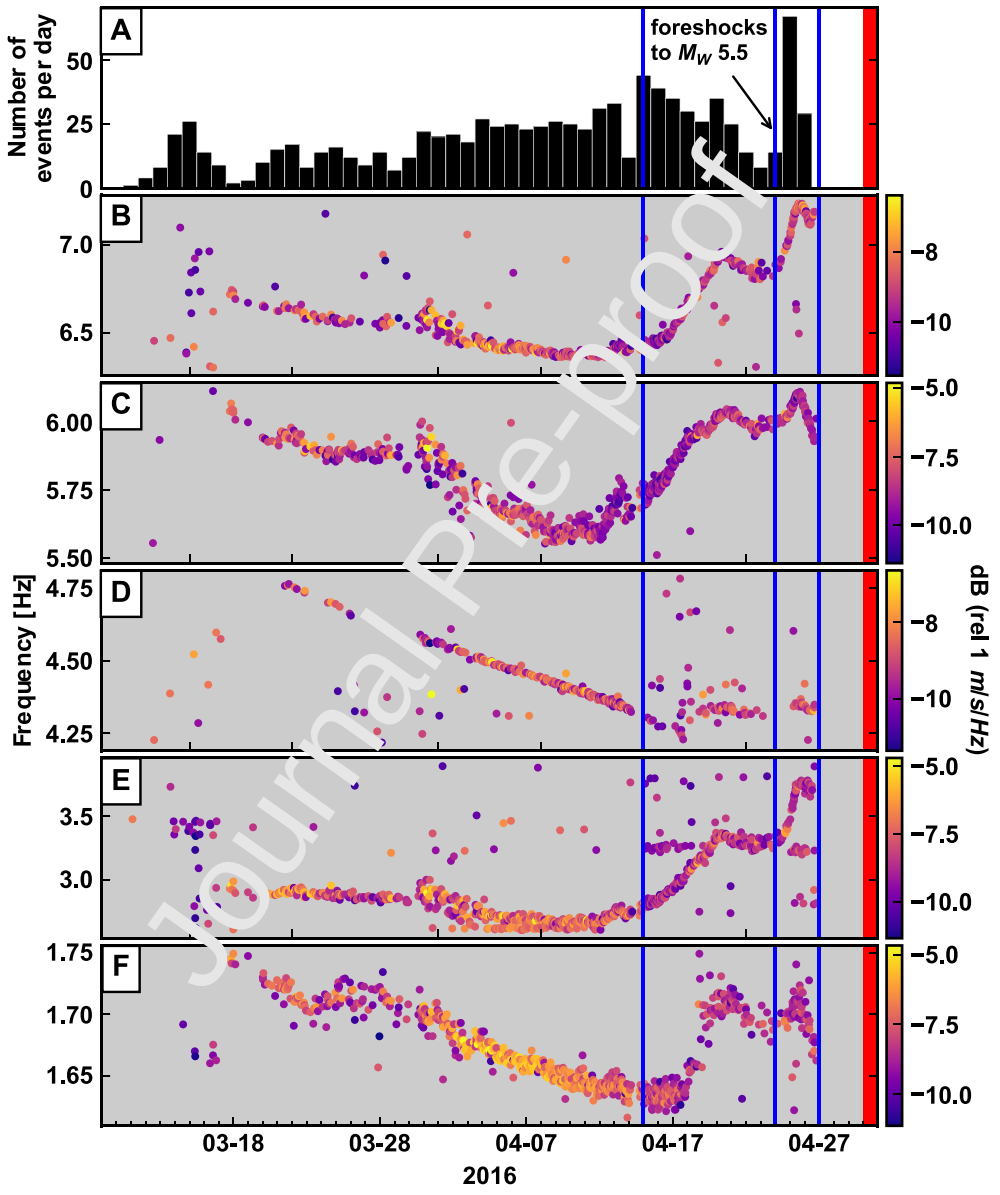

Figure 12: Evolution of the cTOR events spectral peaks during PES III. (A): Number of events per day. (B-F): frequency variation of the first 5 spectral peaks of the coda. Each point represents a peak of each event. The spectral amplitudes of the peaks are represented by a color scale. The solid blue lines indicate VT swarms. The first two are distal swarms (April 15 and 24), while the third one is a proximal swarm (April 27). The vertical red band indicates the eruption phase that began in April 29.

ejected during the violent explosion on October 29, 2014 (de Moor et al., 2016), which was preceded by a PETA period of 34 days.

The observations here provided suggest that the sealing of the hydrothermal system was a recurrent process that leaded to most of the eruptive phases prior to the open-conduit stage. We observe that PETA periods became increasingly longer in duration (Figure 8) which could reflect the progressive opening of the system, since a more open system would require longer duration to over-pressurize. Also, we observe that the magnitude of the PETA tended to decrease, which could mean that required pressure difference to generate the eruption was decreasing due to the progressive opening of the system.

4.2. Precursory seismo-volcanic events: cTOR, LP-HT and LP-T

For the generation of the multitonal resonance typical of cTOR events a closed cavity is required where a high pressure gradient is generated due to a high flow rate (Konstantinou, 2015; Lazio et al., 2019). According to Kumagai and Chouet (2000), the estimated quality factor of 60–80 for a representative cTOR event would correspond to bubbly water or bubbly basalt. We propose that the VLP pulse of cTOR is generated by a slow fluid movement in the shallow magma body. The downward polarity of this pulse could be associated with the rise of a gas pocket in the magmatic column, which causes a downward acceleration of the surrounding fluid. If the fluid is massive enough, it can generate a force that couples to the rock walls during a momentary deflation (Ohai, 1983; Waite, 2015). The escaping mixture of magma and gas from the magma body then produces pressure transients that excite the oscillation of the cavities.

cTOR frequency decrease was the general trend in both PES-III and PES-IV, as observed in other volcanoes (Torres et al., 1996; Molina et al., 2004). This could be due to a variety of factors, such as increase in the fluid density and/or a growth of the cavities or the increase of gas fraction in magma (Kumagai and Chouet, 2001; Molina et al., 2004; Konstantinou, 2015). Despite this general trend, during the two final weeks of PES-III we observe two cycles of frequency increase and decrease. We have already seen that the beginning of each cycle coincides with a VT swarm. In particular, the VT swarm occurring in April 26, 2016 is proximal and no more cTOR were detected after that swarm. Hence, we propose that the first two dVT swarms (April 15 and April 24, 2016, Figure 12) may indicate magma injection events, which in turn could increase degassing and gas temperature in the shallow magma column and, therefore, the acoustic velocity and the frequency of oscillation would also increase. Conversely, the last pVT swarm might be related to the rupture of the hydrothermal system seal, which previously conditioned the cTOR resonances.

Unlike for cTOR events, it was not possible to obtain a source location for LP-HT. However, high attenuation observed at distant stations (VTLA and VTCV) indicate a shallow source. A possibility is that the LP phase is the result of an internal explosion due to the accumulation of gases in the sealed zone of the hydrothermal system (Figure 13B). The consequent HT could be generated by one of multiple processes: acoustic resonance of a fluid-filled fracture (Chouet, 1988); thermoacoustic oscillations (Busse et al., 2005; Montegrossi et al., 2019); Dirac comb effect by sustained repetition of a pressure pulse (Lesage et al., 2006); flow-induced vibrations to the walls of a conduit (Julian, 1994); the excitation of standing waves in a reservoir by flow in a coupled channel (analogous to the clarinet) (Rust et al., 2008); gas flow through a permeable medium (Girona et al., 2019), among others. The observation of period doubling in some LP-HT events (Supplementary Figure S13) points to the flow-induced vibration model (Julian, 1994). Notice that these observations cannot be explained by the shift from matched end (open-open or closed-closed) to mismatched end (open-closed) conditions, or vice versa, in a 1-D resonator since only odd overtones would be observed in the mismatched case. Rust et al. (2008) observed period doubling in an laboratory experiment where air flows up a vertical slit in a gelatin block. Thus, we prefer the interpretation in which the HT phase results from the high-speed flow of the gases in a narrow conduit after being released during the internal explosion (LP phase).

During PES-II (2013) the most important precursor class was the LP-T, which share similarities with LP-HT. We suggest that these two type of event could share the same source but under different conditions. During this stage, the mean RMS amplitude of the tremor phase was 0.19 μm/s for the LP-T and 0.33 μm/s for the LP-HT events. The fact that the amplitudes of the LP-HT were greater than those of the LP-T could indicate that there was an increase in pressure and/or flow velocity that generated the tremor phase, reaching the critical pressure necessary to generate the harmonic signal (Rust et al., 2008). Additionally, the RSEM increased at the same time that the LP-HT events occurred, this could further support the idea of a general pressure increase in the system.

4.3. Interpretation the evolution of the 2010-present eruption

We propose a conceptual model for the 2010-present eruption in Figure 13. This model was derived from the results of this work and the geological and vulcanological information known up to this moment. We will address each stage of the eruption according to this model in next subsections.

4.3.1. Slow reactivation from 1996 to 2009

As we previously mentioned in section 1.2, Turrialba volcano featured signs of unrest possibly dating back to 1980s, but surely since 1996. Inflation of the volcano and VT swarms reflect the early magma intrusion processes (Martini et al., 2010; Soto, 2012). Furthermore, significant increases in low-frequency seismicity were observed during this period (Tassi et al., 2004; Mora et al., 2001; Martini et al., 2010). Finally, the surface conditions also underwent changes such as the increase in the flow and decrease in pH of the magmatic gases (SO_2), as well as the opening of fissures in the walls of the West Crater (Martini et al., 2010) (Figure 13A).

4.3.2. Annual eruptive behaviour from 2010 to 2013

The first five years of eruptive activity at Turrialba volcano comprise 4 main eruptions that occurred at almost annual intervals (Figure 5).

Our seismic records start only a few months prior to the first eruption on January 5, 2010. In this period we observe relatively high RSEM amplitudes (Figure 7A). Among other explanations, the first PETA could reflect the formation of a seal in the hydrothermal system due to mineral precipitation. In this context, a high number of LP-HT signals were generated (Table 1). When the pressure in the seal exceeds the resistance of the rock, an internal explosion occurs (LP phase) and the gas accumulated is released at high speed into a narrow conduit or fissure (HT phase). The late stage of this PETA period was accompanied by pure VT events that reflect brittle rupture in the hydrothermal system (Figure 13B). The process culminated with the opening of the 2010 vent. During this first eruption, the volcano emitted a low content of fresh ash (~5%) (Alvarado et al., 2016a,b), indicating the destruction of pre-existing rock to form the new conduit and the interaction of the shallow magmatic body with the hydrothermal system.

Other minor ash emissions occurred in June, July 2010 and January 2011 (Section 1.2). Before the last one we can observe a PETA (Figure 7A) between November and December 2010. After the first eruption we observe a gradual decrease of the RSEM amplitude, probably related to a relative stabilization of the system after that eruption.

The January 2012 eruption also took place after a PETA (Figure 7A). After this eruption we observe the first few TOR events (Figure 10) indicating the formation of a cavity that can host the oscillation of a fluid at high pressure (Figure 13C). Also, after this eruption we note an small increase in the number of low-magnitude VT events prior, and thus not induced by the Mw 7.6 Nicoya earthquake (September 5, 2012, Figure 9D).

The PETA periods observed previous to the small eruptions of January 2011 and January 2012 show ~1 month temporal separations with their corresponding eruptions Figure 7. This could be interpreted as a delay between the actual seal rupture at depth and the superficial eruptive process.

Additionally, in September 2012 we observe a joint RSEM and SO_2 flux pattern similar to the PETA but that did not result in an eruption (Figure 7B). Instead, at the end of this process, when the amplitude of the RSEM increased in October 2012, we note the earliest observed LP drumbeat sequence (Supplementary Figure S5) which could suggest the repetitive movement of an intruding magma body (Figure 13C) as has been interpreted in the literature (Matoza and Chouet, 2010; Kendrick et al., 2014; Bell et al., 2017).

The May 2013 eruption precursory seismicity was characterized by: a) an overall context of low seismicity (Figure 7B); b) a second drumbeat sequence in March 2013 (Lesage et al., 2018); c) a PETA longer in duration and smaller in magnitude than the prior (Figure 8), and; d) the dominance of LP-T events and only a small proportion of LP-HT. These observations suggest that, among different possible processes, in this case the seal in the hydrothermal system was not very effective, resulting in internal explosions that weren't energetic enough to pressurize the gas that circulates the shallow conduits and was therefore unable to generate the harmonic resonance.

In general, from 2010 to 2013, we can highlight the following facts: a) the RSEM progressively decreased after the first eruption and remained low after 2012; b) the PETA magnitude decreased with each new eruption while its duration became longer (Figure 8); and c) the VT seismic moment decreased until the first half of 2013. These observations reflect, during the first 4 years of activity, how the system progressively decompressed while losing the ability to build up a significant amount of pressure each time it opened a new vent. At the same time, the small magma

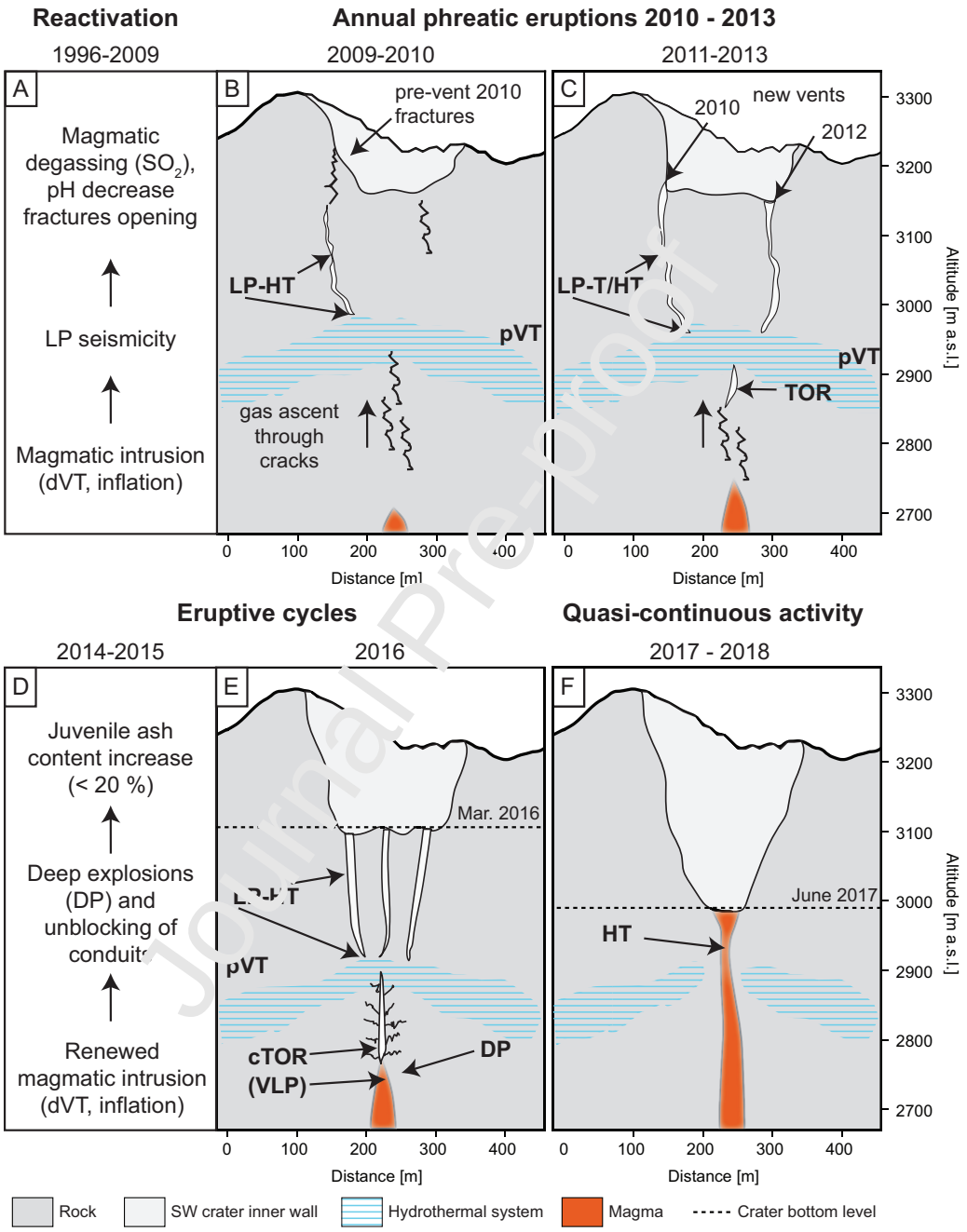

Figure 13: Conceptual model of the evolution of the Turrialba volcano shallow system. The model was conceptualized based on the observations made in this research, together with contributions from other authors mentioned in the text. Each sketch represents a SW-NE cross-section of the southwest active crater. The positions of the crater bottom (horizontal dashed lines in E and F) were obtained by Ruiz et al. (2017) and the date of each measurement is indicated. The positions of both the hydrothermal system and the magma body are approximate. Note that only for pVT and the VLP phase of cTOR events the source locations could be obtained by seismic methods. For LP-T/HT and DP events we speculate about their position based on their characteristics discussed in the text. Acronyms: DP: double-phase event; HT: harmonic tremor; LP-HT: long-period event with harmonic tremor; LP-T: long-period event with tremor; TOR: tornillo-type event; cTOR: compounded tornillo-event; pVT: proximal volcano-tectonic event.

body continued to decompress and rise as reflected by the drumbeat swarm observed in March 2013. Additionally, the decrease of VT seismic moment could reflect the end of the first intrusion that reactivated Turrialba volcano (Figure 9C and D).

4.3.3. Eruptive cycles behaviour from 2014 to 2016

After the 2013 eruption the RSEM level remained low until the end of 2014 (Figure 7B). VT seismicity began to increase progressively since late 2014 (Figure 9D, Figure 13D). Concomitantly, the frequencies of the TOR events increased up to ~10.5 Hz (Figure 10B). During October 2014 a subtle PETA is observed together with a notable decrease on SO_2 flux and a few low amplitude HT episodes (Figure 10). These observations can be interpreted as a greater blocking or sealing of the system, which finally led to the violent eruption on October 29, 2014 as mentioned in section 1.2 (Figure 5D). These observations are in agreement with de Moor et al. (2016) who collected breccia-type ejecta bearing a matrix of hydrothermal minerals (e.g. silica, clays, zeolite) that support the hypothesis of a seal in the hydrothermal system leading to explosive eruptions. The eruptive activity lasted until mid-December, followed by a significant but short increase of VT seismicity (number and magnitude), HT and SO_2 (Figure 7B and Figure 10D-F). This suggests a more open system at the same time that the injection of magma continued.

After the last eruptions in December 2014, a relative calm of around 3 months followed during which RSEM remained low (Figure 7C). Eruptive activity resumed on March 8, 2015, right after the VT events and HT episodes increased (Figure 9D and Figure 10D). The fundamental frequencies (f_1) of the HT episodes were below 1 Hz while TOR events frequencies dropped from 11 to 5 Hz (Figure 10A, B and E). DP events appeared, some of them, associated to eruptions (Figure 13D). The next cycle started on October 16, 2015. In contrast to the previous cycle, it was preceded by a PETA and a notable decrease of the SO_2 emission (Figure 7C). HT episodes had fundamental frequencies (f_1) below 1 Hz (Figure 10D-F). Between the two 2015 cycles seismicity remained relatively low, with only few TOR events and HT episodes. Furthermore, an isolated eruptive event took place on August 15, 2015, preceded by a notable peak of VT seismicity (Figure 9D).

In October occurred the highest number of DP and an increase in the number of TOR events, which had ceased since May of that year (Figure 10). For the latter, the frequencies decreased down to 2 Hz, (Figure 10B) which could indicate, among other explanations, the growth of the resonant cavities and opening of conduits due to the intense interaction between the magmatic gases and the hydrothermal system during the 2014 and 2015 eruptive phases. We interpret that DP events, which commonly accompanied discrete eruptions, were part of this process of opening of the conduits which began at the margin of the rising magma body in interaction with the hydrothermal system (Figure 13E).

Subsequently, during the March to April 2016 PES III, there was an increase in DP events, a high number of cTOR and LP-HT events, and some episodes of harmonic tremor, but in less quantity than in 2015. In this case, the amplitudes, fundamental frequencies and frequency gliding of LP-HT events were lower than in 2009. During PES-I the mean f_1 was 3.2 Hz, while during PES-III it was 1.6 Hz. Assuming the same resonator, this difference could be due to changes in various factors (fluid velocity, resonator geometry, velocity changes in the cavity, etc.). In 2010 the first vent was barely opened (Alvarado et al., 2016a; Elizondo et al., 2019), while in 2016 there were already multiple widened vents. Thus, the frequency decrease could be explained by an increase of the length of the resonator. Similarly, the much lower frequencies of the cTOR (1.6 Hz) than the preceding TOR events (>5 Hz) (Figure 10) could reflect the formation of a larger cavity (Figure 13E). The PETA period associated with this eruption reached the longest duration (Figure 8), suggesting that the system needed a longer time to pressurize because it was almost open. Once the pressure exceeded the resistance of the rocks in the hydrothermal system due to the accumulation of gases, the seal broke releasing the accumulated material (April 27 pVT swarm). The eruptive phase began on April, 29, and continued intermittently until August, 1.

After a pause, a short PETA is observed between September 1 and 13. A new sequence of cTOR occurred during this stage, with frequencies lower than before (~1 Hz, Figure 10) which continued to decrease down to the observed overall minimum (~0.8 Hz) prior to the September 13 eruptive phase onset (Supplementary Figure S11). During the eruptive phase, the RSEM showed relatively high values, comparable to those in 2010 (Figure 7). This activity continued until the end of November when a new short pause occurred. It was precisely during this relative quiescence that the M 5.5 Capellades mainshock occured, on December, 1st 2016 (Linkimer et al., 2018). This sequence represents the climax of the VT activity, both in number and in magnitude (Figure 9).

The moment tensor inversion of the Capellades main shock indicates that the dextral strike-slip double couple component represents 84.5% of the total seismic moment (Linkimer et al., 2018). Although, this observation makes it possible to rule out the significant influence of fluids on the rupture mechanism (Linkimer et al., 2018), fluids can still trigger the rupture via changes in pore pressure or local static stress change. Here we provide several observations reflecting a relationship between the sequence and the volcanic activity that support the idea that this sequence was triggered by the magmatic or hydrothermal fluids:

1. The volume change in the deep magmatic reservoir modeled from deformation data (Müller, 2018; Battaglia et al., 2019) coincides with the one estimated from the seismic moment (Supplementary Figure S6) based on the relationships found by White and McCausland (2016) and Meyer et al. (2021).
2. The position of the deep magma reservoir (Müller, 2018; Battaglia et al., 2019) is aligned in a SW-NE trend with the centroid of the Liebres fault activity (Linkimer et al., 2018) and the active crater of Turrialba volcano.
3. The Liebres fault (Figure 2) (Linkimer et al., 2018) is located between the deep reservoir (5-10 km deep) (Müller, 2018) and the intermediate reservoir (1.65-3.95 km deep) (Ba lilla and Taylor, 2019), at depths similar to that of the intermediate reservoir.
4. A migration of distal seismicity in the SW-NE direction occurred between 2015 and 2017 (Supplementary Figure S5).
5. An increase in cTOR frequencies just after the Capellades foreshock swarm on April, 24.
6. Changes in eruptive activity after the main shock:
   (a) An abrupt increase in fresh content in erupted ash (Supplementary Figure S12).
   (b) Quasi-continuous character of the eruptive activity.
   (c) Frequent strombolian activity (Alvarado et al., 2020).
7. Change in tremor amplitude trend (RSEM, Figure 7). The climatic point occurred during the preceding pre-eruptive period (September to November, 2017). On the other hand, the Capellades main sequence coincides with a PETA, after which a downward trend was sustained until the second half of 2019.
8. An increase in the amount of harmonic tremor, a pronounced increase in its frequencies and sudden decrease in the number of harmonics just after the Capellades mainshock (Figure 10).

These observations support the hypothesis that the Capellades sequence (Linkimer et al., 2018) occurred, at least partially, in response to the stress applied by the magmatic injection. However, the geometry of the Liebres fault might be conditioned by the NNE regional compressive stress in accordance with the dextral fault systems proposed in the literature (Montero and Alvarado, 1995; Montero et al., 2013; Calvo et al., 2019).

4.3.4. Open system and quasi-continuous eruption: 2017 - 2019

The changes detailed above, that occurred in relation to the Capellades sequence, indicate the complete opening of the system. This was confirmed by the observation of an undermining of ~120 m of the active crater, an open conduit evidenced by a magma body at the bottom of the crater from July 2017 to probably May 2018 (Ruiz et al., 2017; Alvarado et al., 2020) and by strombolian activity. The seismo-acoustic signal of the strombolian explosions were DP events (Figure S2), although with lower frequencies the typical values (5-9 Hz), and shorter delays between the seismic and acoustic signal indicating a shallower magma source.

Another VT swarm occured in December 2017 (Figure 9) and was located SW of the Turrialba cone at sea level depth. This swarm culminated with the migration of dVT seismicity that was observed since 2015 with a SW-NE trend (Supplementary Figure S5). At the same time, the amount of harmonic tremor attained a minimum (Figure 10D), after which it increased until reaching its maximum between May and June 2018.

Fundamental frequency changes during this phase could be associated to the magma column level or with variations of the level of exsolution in the magma column (Figure 13F). During 2017, the HT displays its highest fundamental frequency values (Figure 10). This could mean a decrease in the length of the conduit. Then, in April 2018 started a decrease in the fundamental frequency. Inversely, this could indicate that as the magma level descends, the resonator grows and therefore the generation of harmonic tremor increases and its frequency decreases. Also, a change in the gas fraction could be the cause of the frequency changes observed.

4.3.5. Activity decline

During the first semester of 2019, the eruptive activity began to wane and in 2020 only isolated small eruptions occurred between June and July (OVSICORI-UNA, 2021). In addition, between 2019 and the date of writing this paper, a deflation of the Irazú-Turrialba volcanic complex was observed (OVSICORI-UNA, 2021).

5. Conclusions

In this paper we provided the first seismological overview of the recent activity of Turrialba volcano, as early as a few months prior to the first eruptive phase and until its decline in recent years (2019-2020). We analysed more than 11 years of records in order to provide a general description of the opening process of the system after ~150 years of dormancy. The main focus of this work was the identification of precursory signals that could enhance the anticipation of eruptive processes in a surveillance context, as well as the understanding of the geological processes involved.

Our analysis of VT seismicity on the Irazú-Turrialba volcanic complex supports the idea that the main magma reservoir associated with the Turrialba activity is located beneath Irazú volcano. Furthermore, we conclude that, although the Liebres fault geometry might be conditioned by regional tectonic stresses, its triggering resulting in the largest earthquake (M 5.5) in the volcanic complex may have been due to magma dynamics.

The recent eruption (2010-present) of Turrialba volcano has been a long-term process that evolved through different eruptive phases. The pauses between those phases allowed for in-depth observation of different precursory processes for each phase. In the long term, volcanic tremor amplitude decrease was identified as an eruption precursory signal. In total, 9 pre-eruptive tremor abatement (PETA) periods were identified, ranging from 5 to 44 days in duration. Often, PETA periods concurred with a decrease in the SO_2 flux. We interpret these observations a result of the sealing of the hydrothermal system, most probably due to the formation of hydrothermal minerals. Once the system was over-pressurized the seal was breached and the eruption occurred. This process accompanied most of the eruptions previous to the open-conduit phase, and the variations of the PETA features (duration and magnitude) reflect the progressive opening of the system.

In order to better understand the processes ongoing during these periods and to identify short-term precursor signals, we analysed in detail four pre-eruptive stages (PES I-IV). In the short term, the main precursor seismic classes were the LP and tremor events, both harmonic and broadband spectrum (LP-HT and LP-T), compounded tornillo-type events (cTOR) and distal and proximal volcano-tectonic events (dVT and pVT). LP-HT events were observed in three PES (I-III) and the overall evolution of their characteristics reflect the opening of the system. cTOR events were dominant in PES-III and IV.

DP events played an important role in the process of opening the conduits through internal explosions. At first, these explosions showed minor surface expression, probably because the magma was still at depth (e.g. Tameguri et al. (2002) determined initial sources for explosions at Sakurajima volcano to be 2 km deep). Once the system was definitely open in 2017, these explosions showed a Strombolian character. It was during this open-conduit stage that harmonic tremor thrived due to the formation of a resonant conduit fully developed and influenced by the shallow magma body.

Several lines of investigation can be taken in the future to expand our understanding of Turrialba volcano. For example, VT seismicity can be further relocated using double-difference techniques. Quality factor attenuation for TOR and cTOR events must be obtained systematically for each event in the catalog in order to track variations in the fluid involved.

To conclude, we consider that this study contributes to understand the general process of the recent eruption (2010-2021) at Turrialba volcano. Our decadal analysis informs about the slow transition from a closed- to an open-conduit system. Furthermore, our in-depth analysis of pre-eruptive stages provides insights into eruption precursor processes. This new knowledge constitutes valuable information for the volcano monitoring community.

Author contributions

Leonardo van der Laat: Conceptualization, Methodology, Software, Formal Analysis, Investigation, Writing - Original Draft, Visualization; **Mauricio Mora:** Supervision, Conceptualization, Methodology, Software, Formal Analysis, Investigation, Writing - Original Draft, Resources, Funding acquisition, Visualization **Javier Fco. Pacheco:**

Supervision, Conceptualization, Resources, Formal Analysis, Investigation, Funding acquisition, **Philippe Lesage:** Formal Analysis, Writing - Review & Editing; **Esteban Meneses:** Writing - Review & Editing, Funding acquisition.

Acknowledgments

This work was funded by the research project *Red en Sismología Computacional para el Estudio de los Volcanes Activos en Costa Rica* (113-B8-767) and partially from the research project *Implementación de un sistema de monitoreo automático en tiempo real para los volcanes activos de Costa Rica* (113-B9-664) and *Vigilancia Sísmica de Costa Rica* (113-B5-704), all subscribed at the *Vicerrectoría de Investigación, Universidad de Costa Rica*. Part of the work was funded by the research project *Vigilancia de los volcanes de Costa Rica por medio de su actividad sísmica* (SIA 0208-16). We also thank Geoffroy Avard for providing SO_2 and ash data. Seismic instrumentation of the RSN and the OVSICORI is financed by the National Emergency Law No. 8488. We thank the technical staff from RSN (Luis Fernando Brenes and Jean Paul Calvo) and OVSICORI (Christian Garita, Antonio Mata, Daniel Rojas and Hairo Villalobos) for the instrumentation maintenance. L. van der Laat was partially funded by *Centro Nacional de Alta Tecnología* (CeNAT) Scholarship.

References

Alvarado, G.E., Barquero, R., Boschini, I., Chiesa, S., Carr, M.J., 1986. Relación entre la neotectónica y el vulcanismo en Costa Rica. CIAF 11, 246–264.

Alvarado, G.E., Brenes-André, J., Avard, G., Pereira, R., Galve, J.P., Campos Durán, D., de Moor, J.M., Sánchez, R., 2021. La actividad eruptiva del volcán Turrialba (Costa Rica) en el siglo XIX: reinterpretación de los documentos históricos y de los depósitos. Revista Geológica de América Central , 1–41.

Alvarado, G.E., Brenes-André, J., Barrantes, M., Vega, E., De Moor, J.M., Avard, G., Dellino, P., Mele, D., Devitre, C., Piazza, A., Rizzo, A., 2016a. La actividad explosiva del volcán Turrialba (Costa Rica) en el período 2010 - 2016. Revista Geológica de América Central 55, 7–60. doi:10.15517/rgac.v55i0.26965.

Alvarado, G.E., Esquivel, L., Sánchez, B., Matamoros, G., 2020. Peligro volcánico de Turrialba, Costa Rica. Technical Report. Comisión Nacional de Prevención de Riesgos y Atención de Emergencias (CNE). San José, Costa Rica.

Alvarado, G.E., Mele, D., Dellino, P., de Moor, J.M., Avard, G., 2016b. Are the ashes from the latest eruptions (2010–2016) at Turrialba volcano (Costa Rica) related to phreatic or phreatomagmatic events? Journal of Volcanology and Geothermal Research 327, 407–415. doi:10.1016/j.jvolgeores.2016.09.003.

Avard, G., Pacheco, J.F., Fernández, E., Martínez, M., Menjívar, E., Brenes, J., van der Laat, R., Duarte, E., Sáenz, W., 2012. Turrialba volcano: Opening of a new fumarolic vent on the southeast flank of the West Crater on January 12th, 2012, as consequence of shallow decompression. Technical Report. Observatorio Vulcanológico y Sismológico de Costa Rica, Universidad Nacional. Heredia, Costa Rica.

Avard, G., Pacheco, J.F., Martínez, M., Sáenz, W., 2013. Reporte técnico: Emisión de cenizas al volcán Turrialba el 21 de mayo del 2013. Technical Report. Observatorio Vulcanológico y Sismológico de Costa Rica Universidad Nacional (OVSICORI-UNA).

Badilla, D., Taylor, W., 2019. Perfil de magnetotelúrica en el volcán Turrialba, in: 3er Congreso Geológico, Universidad de Costa Rica, San José, Costa Rica. p. 35.

Barquero, R., Alvarado, G.E., 1989. Los enjambres de temblores en el arco volcánico de Costa Rica. Technical Report.

Battaglia, M., Alpala, J., Alpala, R., Angarita, M., Arcos, D., Euillades, L., Euillades, P., Muller, C., Narváez, L., 2019. Monitoring Volcanic Deformation, in: Reference Module in Earth Systems and Environmental Sciences, pp. 1–42. doi:10.1016/b978-0-12-409548-9.10902-9.

Bean, C.J., De Barros, L., Lokmer, I., Métaxian, J.P., O'Brien, G., Murphy, S., 2014. Long-period seismicity in the shallow volcanic edifice formed from slow-rupture earthquakes. Nature Geoscience 7, 71–75. doi:10.1038/ngeo2027.

Bell, A.F., Hernandez, S., Gaunt, H.E., Mothes, P., Ruiz, M., Sierra, D., Aguaiza, S., 2017. The rise and fall of periodic 'drumbeat' seismicity at Tungurahua volcano, Ecuador. Earth and Planetary Science Letters 475, 58–70. doi:10.1016/j.epsl.2017.07.030.

Benoit, J.P., McNutt, S.R., 1997. New constraints on source processes of volcanic tremor at Arenal Volcano, Costa Rica, using broadband seismic data. Geophysical Research Letters 24, 449–452. doi:10.1029/97GL00179.

Beyreuther, M., Barsch, R., Krischer, L., Megies, T., Behr, Y., Wassermann, J., 2010. ObsPy: A python toolbox for seismology. Seismological Research Letters 81. doi:10.1785/gssrl.81.3.530.

Busse, F.H., Monkewitz, P.A., Hellweg, M., 2005. Are harmonic tremors self-excited thermoacoustic oscillations? Earth and Planetary Science Letters 240, 302–306. doi:10.1016/j.epsl.2005.09.046.

Calvo, C., Madrigal, K., Merayo, F., Salazar, M., Fallas, C., Alvarado, G.E., Sánchez, B., Sánchez, R., 2019. Modelo volcanotectónico del graben cuspidal complejo del Turrialba (Costa Rica) y su relación con los colapsos sectoriales bajo un régimen transpresivo y transtensivo. Revista Geológica de América Central 61, 57–77.

Caudron, C., Taisne, B., Neuberg, J., Jolly, A.D., Christenson, B., Lecocq, T., Suparjan, Syahbana, D., Suantika, G., 2018. Anatomy of phreatic eruptions. Earth, Planets and Space doi:10.1186/s40623-018-0938-x.

Chiodini, G., Giudicepietro, F., Vandemeulebrouck, J., Aiuppa, A., Caliro, S., De Cesare, W., Tamburello, G., Avino, R., Orazi, M., D'Auria, L., 2017. Fumarolic tremor and geochemical signals during a volcanic unrest. Geology 45. doi:10.1130/G39447.1.

Chouet, B.A., 1988. Resonance of a fluid-driven crack: radiation properties and implications for the source of long-period events and harmonic tremor. Journal of Geophysical Research 93, 4375–4400. doi:10.1029/JB093iB05p04375.

Chouet, B.A., Dawson, P.B., 2016. Origin of the pulse-like signature of shallow long-period volcano seismicity. Journal of Geophysical Research: Solid Earth 121, 5931–5941. doi:10.1002/2016JB013152.

Conde, V., Robidoux, P., Avard, G., Galle, B., Aiuppa, A., Muñoz, A., Giudice, G., 2014. Measurements of volcanic SO 2 and CO 2 fluxes by combined DOAS, Multi-GAS and FTIR observations: a case study from Turrialba and Telica volcanoes. International Journal of Earth Sciences 103, 2335–2347. doi:10.1007/s00531-014-1040-7.

De la Cruz-Reyna, S., Reyes-Dávila, G.A., 2001. A model to describe precursory material-failure phenomena: Applications to short-term forecasting at Colima volcano, Mexico. Bulletin of Volcanology 63, 297–308. doi:10.1007/s004450100152.

Denyer, P., Aguilar, T., Montero, W., 2014. Cartografía geológica de la península de Nicoya, Costa Rica: estratigrafía y tectónica. Editorial UCR, San José, Costa Rica.

DeVitre, C.L., Gazel, E., Allison, C.M., Soto, G., Madrigal, P., Alvarado, G.E., Lücke, O.H., 2019. Multi-stage chaotic magma mixing at Turrialba volcano. Journal of Volcanology and Geothermal Research 381, 330–346. doi:10.1016/j.jvolgeores.2019.06.011.

Di Piazza, A., Vona, A., Mollo, S., De Astis, G., Soto, G.J., Romano, C., 2019. Unsteady magma discharge during the "El Retiro" subplinian eruption (Turrialba volcano, Costa Rica): Insights from textural and petrological analyses. Journal of Volcanology and Geothermal Research 371, 101–115.

Dmitrieva, K., Hotovec-Ellis, A.J., Prejean, S., Dunham, E.M., 2013. Frictional-faulting model for harmonic tremor before Redoubt Volcano eruptions. Nature Geoscience 6, 652–656. doi:10.1038/ngeo1879.

Elizondo, V., Alvarado, G.E., Soto, D., 2019. Evolución espacio-temporal de las bocas eruptivas de los volcanes Irazú, Arenal, Turrialba y Poás en el tiempo histórico (Costa Rica). Revista Geológica de América Central 61, 35–55.

Eyre, T.S., Bean, C.J., De Barros, L., O'Brien, G.S., Martini, F., Lokmer, I., Mora, M.M., Pacheco, J.F., Soto, G.J., 2013. Moment tensor inversion for the source location and mechanism of long period (LP) seismic events from 2009 at Turrialba volcano, Costa Rica. Journal of Volcanology and Geothermal Research 258, 215–223. doi:10.1016/j.jvolgeores.2013.04.016.

Fazio, M., Alparone, S., Benson, P.M., Cannata, A., Vinciguerra, S., 2019. Genesis and mechanisms controlling tornillo seismo-volcanic events in volcanic areas. Scientific Reports 9. doi:10.1038/s41598-019-43842-y.

Fernández, M., Mora, M.M., Barquero, R., 1998. Los procesos sísmicos en el volcán Irazú (Costa Rica). Revista Geológica de América Central , 47–59.

Gazel, E., Flores, K.E., Carr, M.J., 2021. Architectural and tectonic controls on the segmentation of the central american volcanic arc. doi:10.1146/annurev-earth-082420-055108.

Geirsson, H., Rodgers, M., LaFemina, P., Witter, M., Roman, D., Muñoz, A., Tenorio, V., Alvarez, J., Jacobo, V.C., Nilsson, D., Galle, B., Feineman, M.D., Furman, T., Morales, A., 2014. Multidisciplinary observations of the 2011 explosive eruption of Telica volcano, Nicaragua: Implications for the dynamics of low-explosivity ash eruptions. Journal of Volcanology and Geothermal Research 271, 55–69. doi:10.1016/j.jvolgeores.2013.11.009.

Girona, T., Caudron, C., Huber, C., 2019. Origin of Shallow Volcanic Tremor: The Dynamics of Gas Pockets Trapped Beneath Thin Permeable Media. Journal of Geophysical Research: Solid Earth doi:10.1029/2019JB017482.

Güendel, F., 1984. Enjambres sísmicos en el volcán Irazú. Technical Report. OVSICORI-UNA. Heredia, Costa Rica.

Hagerty, M., Schwartz, S.Y., Garcés, M.A., Protti, M., 2000. Analysis of seismic and acoustic observations at Arenal Volcano, Costa Rica, 1995–1997. Journal of Volcanology and Geothermal Research 101, 27–65. doi:https://doi.org/10.1016/S0377-0273(00)00162-1.

Hilton, D.R., Ramírez, C.J., Mora-Amador, R., Fischer, T.P., Füri, E., Barry, P.H., Shaw, A.M., 2010. Monitoring of temporal and spatial variations in fumarole helium and carbon dioxide characteristics at Poás and Turrialba Volcanoes, Costa Rica (2001-2009). Geochemical Journal 44, 431–440. doi:10.2343/geochemj.1.0085.

Hotovec, A.J., Prejean, S.G., Vidale, J.E., Gomberg, J., 2013. Strongly gliding harmonic tremor during the 2009 eruption of Redoubt Volcano. Journal of Volcanology and Geothermal Research 259, 89–99. doi:10.1016/j.jvolgeores.2012.01.001.

Hotovec-Ellis, A.J., Jeffries, C., 2016. Near Real-time Detection, Clustering, and Analysis of Repeating Earthquakes: Application to Mount St. Helens and Redoubt Volcanoes, in: Seismological Society of America Annual Meeting, Seismological Society of America Annual Meeting. Seismological Society of America Annual Meeting, Reno, Nevada.

Imai, H., 1983. Experimental study on mechanism of implosion earthquakes during the 1973 successive eruptive activity of Asama volcano. Bulletin of the Earthquake Research Institute, University of Tokyo 58.

Jiwani-Brown, E.A., Planes, T., Pacheco, J.F., Mora, M.M., Lupi, M., 2020. Using ambient noise tomography to image tectonic and magmatic features of the Irazú-Turrialba volcanic complex at regional and local scales, in: EGU General Assembly 2020. doi:10.5194/egusphere-egu2020-17795.

Julian, B.R., 1994. Volcanic tremor: nonlinear excitation by fluid flow. Journal of Geophysical Research 99. doi:10.1029/93jb03129.

Kendrick, J.E., Lavallée, Y., Hirose, T., Di Toro, G., Hornby, A.J., De Angelis, S., Dingwell, D.B., 2014. Volcanic drumbeat seismicity caused by stick-slip motion and magmatic frictional melting. Nature Geoscience 7, 438–442. doi:10.1038/ngeo2146.

Konstantinou, K.I., 2015. Tornillos modeled as self-oscillations of fluid filling a cavity: Application to the 1992-1993 activity at Galeras volcano, Colombia. Physics of the Earth and Planetary Interiors doi:10.1016/j.pepi.2014.10.014.

Kumagai, H., Chouet, B.A., 2000. Acoustic properties of a crack containing magmatic or hydrothermal fluids. Journal of Geophysical Research: Solid Earth 105, 25493–25512. doi:10.1029/2000jb900273.

Kumagai, H., Chouet, B.A., 2001. The dependence of acoustic properties of a crack on the resonance mode and geometry. Geophysical Research Letters 28, 3325–3328. doi:10.1029/2001GL013025.

van der Laat, L., 2020. Análisis de los precursores sísmicos de los periodos eruptivos de 2010, 2013 y 2016 en el volcán Turrialba, Costa Rica, Bachelor's thesis. Universidad de Costa Rica , 1–155.

van der Laat, L., Linkimer, L., 2019. La sismicidad tectónica en el edificio del volcán Turrialba durante el 2016, in: 3er Congreso Geológico, Universidad de Costa Rica, San José, Costa Rica. URL: http://geologia.ucr.ac.cr/descarga-de-documentos.html?view=download&id=38.

van der Laat, L., Mora, M.M., 2017. Evolución de las señales de largo período seguidos de tremor armónico; registrados antes de la erupción del 4 de enero de 2010 y la secuencia eruptiva del 2016; volcán Turrialba (Costa Rica), in: I Congreso Centroamericano de Ciencias de la Tierra, San

José, Costa Rica. pp. –. URL: http://www.tierraymar.una.ac.cr/cctm2017/index.php.
van der Laat, L., Mora, M.M., Pacheco, J.F., Cornejo-Suárez, G., 2018. Evolution of Harmonic Tremor Coda Associated to LP Events Recorded Previous to the January 4th, 2010, Eruption and 2016 Eruptive Cycle at Turrialba volcano (Costa Rica), in: 2018 Seismology of the Americas Meeting, Latin American and Caribbean Seismological Comission, Seismological Society of America, p. 829. URL: https://www.seismosoc.org/wp-content/uploads/2018/09/SSA_LACSC-Program-2018.pdf.
LaFemina, P., Dixon, T.H., Govers, R., Norabuena, E., Turner, H., Saballos, A., Mattioli, G., Protti, M., Strauch, W., 2009. Fore-arc motion and Cocos Ridge collision in Central America. Geochemistry, Geophysics, Geosystems 10. doi:10.1029/2008GC002181.
Lesage, P., 2008. Automatic estimation of optimal autoregressive filters for the analysis of volcanic seismic activity. Natural Hazards and Earth System Science 8, 369–376. doi:10.5194/nhess-8-369-2008.
Lesage, P., 2009. Interactive Matlab software for the analysis of seismic volcanic signals. Computers and Geosciences 35, 2137–2144. doi:10.1016/j.cageo.2009.01.010.
Lesage, P., Mora, M.M., Alvarado, G.E., Pacheco, J., Métaxian, J.P., 2006. Complex behavior and source model of the tremor at Arenal volcano, Costa Rica. Journal of Volcanology and Geothermal Research 157, 49–59. doi:10.1016/j.jvolgeores.2006.03.047.
Lesage, P., Muzellec, T., Mora, M.M., Pacheco, J.F., 2018. Observation and preliminary analysis of drumbeat seismicity at Turrialba volcano, Costa Rica, in: Cities on Volcanoes, p. 842. URL: http://editoria.rm.ingv.it/miscellanea/2018/miscellanea43/.
Linkimer, L., 2003. Neotectónica del extremo oriental del Cinturón Deformado del Centro de Costa Rica, Bachelor's thesis. Universidad de Costa Rica , 103.
Linkimer, L., Arroyo, I.G., Soto, G.J., Porras, J.L., Araya, M.C., Mora, M.M., Taylor, M., 2015. El sismo de Capellades del 2016 y su secuencia sísmica: Manifestación de fallamiento de rumbo en el arco volcánico de Costa Rica. Boletín de Geología 40, 35–53.
Lücke, O.H., Götze, H.J., Alvarado, G.E., 2010. A constrained 3D density model of the upper crust from gravity data interpretation for central Costa Rica. International Journal of Geophysics 2010. doi:10.1155/2010/860902.
Lupi, M., Fuchs, F., Pacheco, J.F., 2014. Fault reactivation due to the M7.6 Nicoya earthquake at the Turrialba-Irazú volcanic complex, Costa Rica: Effects of dynamic stress triggering. Geophysical Research Letters 41. doi:10.1002/2014GL059942.
Martínez, M., Pacheco, J.F., 2011. Informe sobre reporte de caída de ceniza en las inmediaciones del poblado La Central Volcán Turrialba. Technical Report. Observatorio Vulcanológico y Sismológico de Costa Rica Universidad Nacional (OVSICORI-UNA). Heredia, Costa Rica.
Martini, F., Tassi, F., Vaselli, O., Del Potro, R., Martinez, M., van der Laat, R., Fernandez, E., 2010. Geophysical, geochemical and geodetical signals of reawakening at Turrialba volcano (Costa Rica) after almost 150years of quiescence. Journal of Volcanology and Geothermal Research 198, 416–432. doi:10.1016/j.jvolgeores.2010.09.021.
Matoza, R.S., Chouet, B.A., 2010. Subevents of long-period seismicity: Implications for hydrothermal dynamics during the 2004-2008 eruption of Mount St. Helens. Journal of Geophysical Research: Solid Earth 115. doi:10.1029/2010JB007839.
Meyer, K., Biggs, J., Aspinall, W., 2021. A Bayesian reassessment of the relationship between seismic moment and magmatic intrusion volume during volcanic unrest. Journal of Volcanology and Geothermal Research 419. doi:10.1016/j.jvolgeores.2021.107375.
Molina, I., Kumagai, H., Yepes, H., 2004. Resonance of a volcanic conduit triggered by repetitive injections of an ash-laden gas. Geophysical Research Letters 31, 2–5. doi:10.1029/2003GL018634.
Montegrossi, G., Farina, A., Fusi, L., De Biase, A., 2019. Mathematical model for volcanic harmonic tremors. Scientific Reports 9. doi:10.1038/s41598-019-50675-2.
Montero, W., Alvarado, G.E., 1995. El terremoto de Patillos del 30 de diciembre de 1952 (Ms = 5,9) y el contexto neotectónico de la región del volcán Irazú, Costa Rica. Revista Geológica de América Central 18, 25–42.
Montero, W., Rojas, W., Linkimer, L., 2013. Neotectónica de las fallas Ochomogo y Capellades y su relación con el sistema de falla Aguacaliente, falda sur del macizo Irazú-Turrialba, Costa Rica. Revista Geológica de América Central2 48, 119–139.
de Moor, J.M., Aiuppa, A., Pacheco, J., Avard, G., Kern, C., Liuzzo, M., Martínez, M., Giudice, G., Fischer, T.P., 2016. Short-period volcanic gas precursors to phreatic eruptions: Insights from Poás Volcano, Costa Rica. Earth and Planetary Science Letters 442. doi:10.1016/j.epsl.2016.02.056.
Mora, M., 2003. Étude de la structure superficielle et de l'activité sismique du volcan Arenal, Costa Rica. Ph.D. thesis. Université de Savoie. France.
Mora, M., 2016. Informe de avance sobre la actividad sísmica y eruptiva del volcán Turrialba (Costa Rica): Abril-mayo de 2016. Technical Report. Red Sismológica Nacional (RSN: UCR-ICE). San José, Costa Rica.
Mora, M., Alvarado, G.E., 2016. Actividad del volcán Turrialba Periodo: 30 de abril - 03 de mayo del 2016. Technical Report. Red Sismológica Nacional (RSN: UCR-ICE). San José, Costa Rica. URL: https://rsn.ucr.ac.cr/actividad-volcanica/reportes-volcanicos/6530-03-05-16-actividad-del-volcan-turrialba-del-30-de-abril-al-3-de-mayo-del-2016.
Mora, M., van der Laat, L., Pacheco, J.F., 2019. Variaciones temporales de las características espectrales del tremor armónico del volcán Turrialba (Costa Rica): 2009-2018, in: 3er Congreso Geológico, Universidad de Costa Rica, San José, Costa Rica. p. 70. URL: http://geologia.ucr.ac.cr/descarga-de-documentos.html?view=download&id=38.
Mora, M., Rojas, W., Linkimer, L., 2001. Resultados de una campaña sismológica realizada del 12 al 14 de marzo del 2001 en el volcán Turrialba, Costa Rica. Technical Report. Red Sismológica Nacional (RSN: UCR-ICE). San José, Costa Rica.
Mora, M., Soto, G., 2016. Resumen de la actividad sísmica y eruptiva del volcán Turrialba. Technical Report. Red Sismológica Nacional (RSN: UCR-ICE). San José, Costa Rica.
Mora, M.M., Pacheco, J.F., 2018. Evolución del tremor armónico del volcán Turrialba (Costa Rica) durante el periodo 2010-2018, in: 2do Minicongreso Geológico, Universidad de Costa Rica, San José, Costa Rica. p. 39.
Müller, C., 2018. 2015-2016 Turrialba deformation observed by GPS measurements. Technical Report. OVSICORI. Heredia, Costa Rica.
Nishimura, T., Iguchi, M., Yakiwara, H., Oikawa, J., Kawaguchi, R., Aoyama, H., Nakamichi, H., Ohta, Y., Tameguri, T., 2013. Mechanism of small vulcanian eruptions at Suwanosejima volcano, Japan, as inferred from precursor inflations and tremor signals. Bulletin of Volcanology 75, 1–12. doi:10.1007/s00445-013-0779-1.
Noll, A.M., 1967. Cepstrum Pitch Determination. The Journal of the Acoustical Society of America 41, 293–309. doi:10.1121/1.1910339.
O'Connor, J.M., Stoffers, P., Wijbrans, J.R., Worthington, T.J., 2007. Migration of widespread long-lived volcanism across the Galápagos Volcanic

Province: Evidence for a broad hotspot melting anomaly? Earth and Planetary Science Letters 263. doi:10.1016/j.epsl.2007.09.007.
OVSICORI-UNA, 2021. Boletín anual del Programa de Vigilancia Volcánica, Año 2020. Technical Report. Observatorio Vulcanológico y Sismológico de Costa Rica, Universidad Nacional. Heredia, Costa Rica. URL: http://www.ovsicori.una.ac.cr/index.php/descargas/category/64-boletines-semanales-vulcanologia-2020?download=854:boletin-anual-del-programa-de-vigilancia-volcanica-ano-2020.
Pacheco, J.F., 2018. Narigones del volcán Turrialba: Partición de energía sónica y sísmica, in: 2do Minicongreso Geológico, San José. p. 45.
Quintero, R., Kissling, E., 2001. An improved P-wave velocity reference model for Costa Rica. Geofisica Internacional 40. doi:10.22201/igeof.00167169p.2001.40.1.416.
Reagan, M., Duarte, E., Soto, G.J., Fernández, E., 2006. The eruptive history of Turrialba volcano, Costa Rica, and potential hazards from future eruptions. Special Paper of the Geological Society of America 412, 235–257. doi:10.1130/2006.2412(13).
Rodgers, M., Roman, D.C., Geirsson, H., LaFemina, P., McNutt, S.R., Muñoz, A., Tenorio, V., 2015. Stable and unstable phases of elevated seismic activity at the persistently restless Telica Volcano, Nicaragua. Journal of Volcanology and Geothermal Research 290, 63–74. doi:10.1016/j.jvolgeores.2014.11.012.
Roman, D.C., Rodgers, M., Geirsson, H., LaFemina, P.C., Tenorio, V., 2016. Assessing the likelihood and magnitude of volcanic explosions based on seismic quiescence. Earth and Planetary Science Letters 450, 20–28. doi:10.1016/j.epsl.2016.06.020.
Ruiz, P., Turrin, B., Soto, G., del Potro, R., Gagnevin, D., Gazel, E., Mora, M., Carr, J., Swisher, C., 2010. Unveiling Turrialba (Costa Rica) volcano's latest geological evolution through new 40Ar/39Ar, ages, in: AGU Fall Meeting Abstracts.
Ruiz, P., Vega, P., Mora, M.M., Soto, G.J., Martínez, D., Barrantes, R., 2017. Geomorphological mapping using drones into the eruptive summit of Turrialba volcano, Costa Rica., in: AGU Fall Meeting.
Rust, A.C., Balmforth, N.J., Mandre, S., 2008. The feasibility of generating low-frequency volcano seismicity by flow through a deformable channel. Geological Society Special Publication 307, 45–56. doi:10.1144/SP307.4.
Ryan, W.B.F., Carbotte, S.M., Coplan, J.O., O'Hara, S., Melkonian, A., Arko, R., Weissel, R.A., Ferrini, V., Goodwillie, A., Nitsche, F., Bonczkowski, J., Zemsky, R., 2009. Global Multi-Resolution Topography synthesis. Geochemistry, Geophysics, Geosystems 10. doi:10.1029/2008GC002332.
Savitzky, A., Golay, M.J., 1964. Smoothing and Differentiation of Data by Simplified Least Squares Procedures. Analytical Chemistry 36. doi:10.1021/ac60214a047.
Soto, G.J., 1988. Estructuras volcano-tectónicas del volcán Turrialba, Costa Rica, América Central, in: V Congreso Geológico Chileno, Departamento de Geología y Geofísica, Universidad de Chile, Santiago. pp. 63–75.
Soto, G.J., 2012. Preparación de mapas de peligros volcánicos y restricción de uso de la tierra en el volcán Turrialba. Technical Report. FUNDEVI, Universidad de Costa Rica.
Soto, G.J., Mora, M.M., 2012. Actividad del Volcán Turrialba en el periodo 2007-2011 y perspectivas de su amenaza volcánica, in: Desastres: Costa Rica en el tercer milenio desafíos y propuestas para la reducción de vulnerabilidad. chapter 12, pp. 287–310.
Stix, J., de Moor, J.M., 2018. Understanding and forecasting phreatic eruptions driven by magmatic degassing. Earth, Planets and Space 70. doi:10.1186/s40623-018-0855-z.
Tameguri, T., Iguchi, M., Ishihara, K., 2002. Mechanism of Explosive Eruptions from Moment Tensor Analyses of Explosion Earthquakes at Sakurajima Volcano, Japan. Bulletin of the Volcanological Society of Japan 47.
Tassi, F., Vaselli, O., Barboza, V., Fernandez, E., Duarte, E., 2004. Fluid geochemistry and seismic activity in the period of 1998-2002 at Turrialba Volcano (Costa Rica). Annals of Geophysics 47, 1501–1511. doi:10.4401/ag-3355.
Thun, J., Lokmer, I., Bean, C.J., 2015. New observations of displacement steps associated with volcano seismic long-period events, constrained by step table experiments. Geophysical Research Letters 42, 3855–3862. doi:10.1002/2015GL063924.
Torres, R.A., Gómez M., D.M., Narváez, M.L., 1996. Unusual seismic signals associated with the activity at Galeras volcano, Colombia, from July 1992 to September 1994. Annali di Geofisica 39, 299–310. doi:10.4401/ag-3975.
Vaselli, O., Tassi, F., Duarte, E., Fernandez, E., Poreda, R.J., Huertas, A.D., 2010. Evolution of fluid geochemistry at the Turrialba volcano (Costa Rica) from 1998 to 2008. Bulletin of Volcanology 72, 397–410. doi:10.1007/s00445-009-0332-4.
Von Huene, R., Bialas, J., Flueh, E., Cropp, B., Csernok, T., Fabel, E., Hoffmann, J., Emeis, K., Holler, P., Jeschke, G., Leandro M., C., Fernandéz, I.P., Chavarria S., J., Florez H., A., Escobedo Z., D., León, R., Barrios L., O., 1995. Morphotectonics of the Pacific convergent margin of Costa Rica. Special Paper of the Geological Society of America 295. doi:10.1130/SPE295-p291.
Waite, G.P., 2015. Very-Long-Period Seismicity at Active Volcanoes: Source Mechanisms. doi:10.1007/978-3-642-35344-4{_}46.
Werner, R., Hoernle, K., Van Den Bogaard, P., Ranero, C., Von Huene, R., Korich, D., 1999. Drowned 14-m.y.-old Galapagos archipelago off the coast of Costa Rica: Implications for tectonic and evolutionary models. Geology 27. doi:10.1130/0091-7613(1999)027<0499:DMYOGP>2.3.CO;2.
White, R., McCausland, W., 2016. Volcano-tectonic earthquakes: A new tool for estimating intrusive volumes and forecasting eruptions. Journal of Volcanology and Geothermal Research 309, 139–155. doi:10.1016/j.jvolgeores.2015.10.020.
Zecevic, M., De Barros, L., Eyre, T.S., Lokmer, I., Bean, C.J., 2016. Relocation of long-period (LP) seismic events reveals en echelon fractures in the upper edifice of Turrialba volcano, Costa Rica. Geophysical Research Letters 43, 105–10. doi:10.1002/2016GL070427.

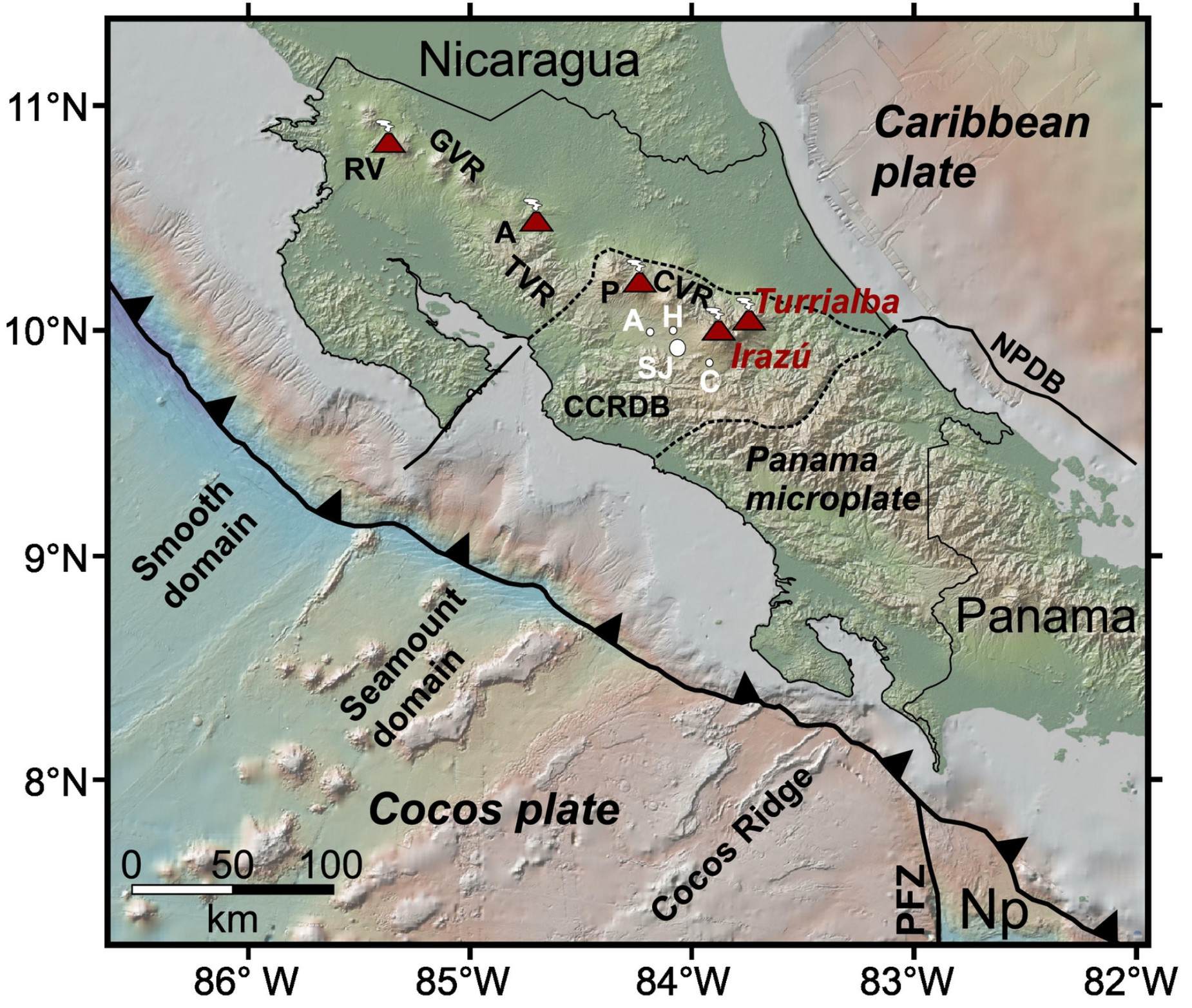
Nicaragua
Caribbean plate
RV
GVR
A
TVR
P
CVR
Turrialba
A
H
SJ
C
Irazú
CCRDB
NPDB
Panama microplate
Panama
Smooth domain
Seamount domain
Cocos plate
Cocos Ridge
PFZ
Np
0 50 100
km
11°N
10°N
9°N
8°N
86° W
85°W
84°W
83°W
82°W

Figure 1

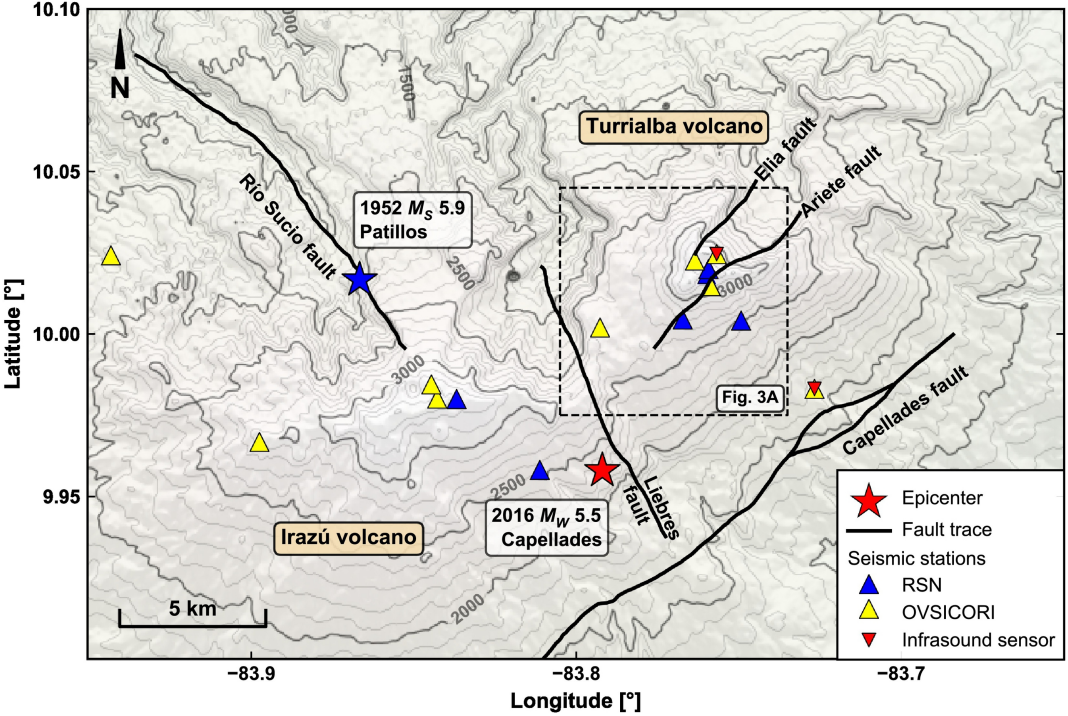
N
Turrialba volcano
Río Sucio fault
1952 M_S 5.9
Patillos
Elía fault
Ariete fault
Fig. 3A
Capellades fault
Liebres fault
2016 M_W 5.5
Capellades
Irazú volcano
5 km
1500
2000
2500
3000
Epicenter
Fault trace
Seismic stations
RSN
OVSICORI
Infrasound sensor
10.10
10.05
10.00
9.95
Latitude [°]
−83.9
−83.8
−83.7
Longitude [°]

Figure 2

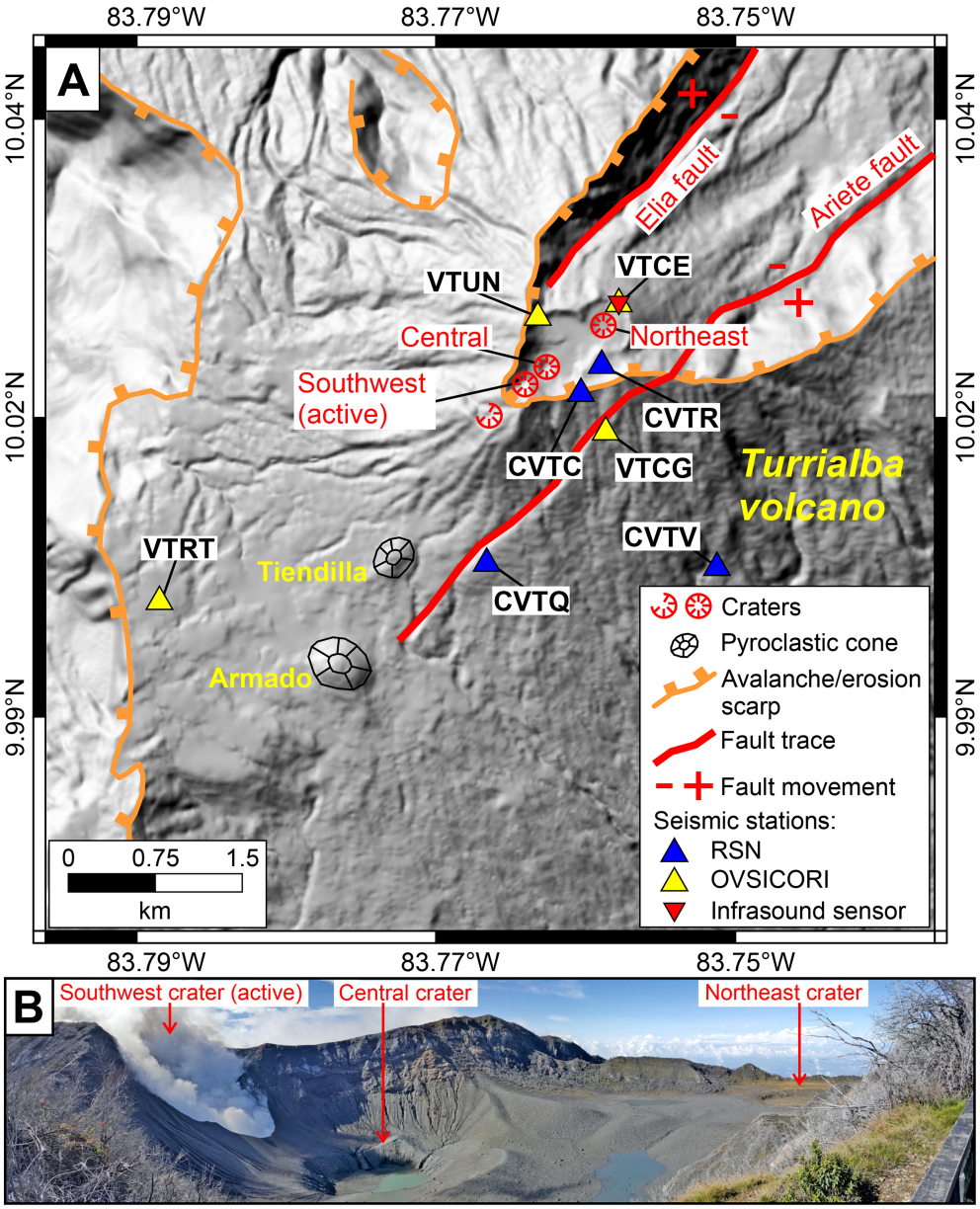
A
83.79°W
83.77°W
83.75°W
10.04°N
10.02°N
9.99°N
Elia fault
Ariete fault
VTUN
VTCE
Central
Northeast
Southwest
(active)
CVTR
CVTC
VTCG
Turrialba
volcano
CVTV
VTRT
Tiendilla
CVTQ
Armado
Craters
Pyroclastic cone
Avalanche/erosion scarp
Fault trace
Fault movement
Seismic stations:
RSN
OVSICORI
Infrasound sensor
0
0.75
1.5
km

B
Southwest crater (active)
Central crater
Northeast crater

Figure 3

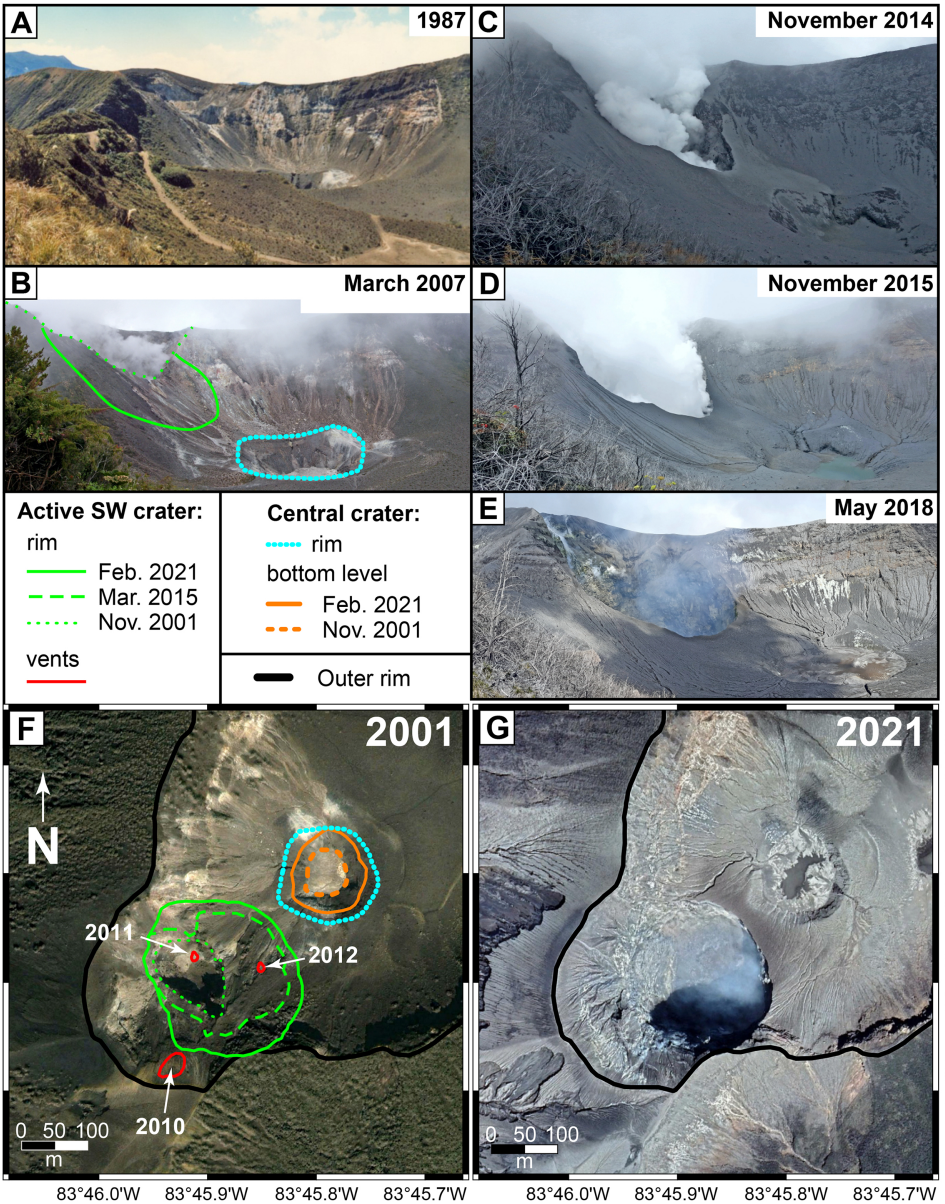
A
1987
C
November 2014
B
March 2007
D
November 2015
E
May 2018
Active SW crater:
rim
Feb. 2021
Mar. 2015
Nov. 2001
vents
Central crater:
rim
bottom level
Feb. 2021
Nov. 2001
Outer rim
F
2001
N
2011
2012
2010
0 50 100
m
G
2021
0 50 100
m
10°1.3'N
10°1.2'N
10°1.1'N
10°1.0'N
83°46.0'W
83°45.9'W
83°45.8'W
83°45.7'W

Figure 4

2010
2011
2012
2013
2014
2015
2016
2017
2018
2019
2020
2021
~annual isolated eruptive events
eruptive cycles
open vent:
quasi-continuous
eruptive activity
Decline
A
B
C
D
E
F
G
H

Figure 5

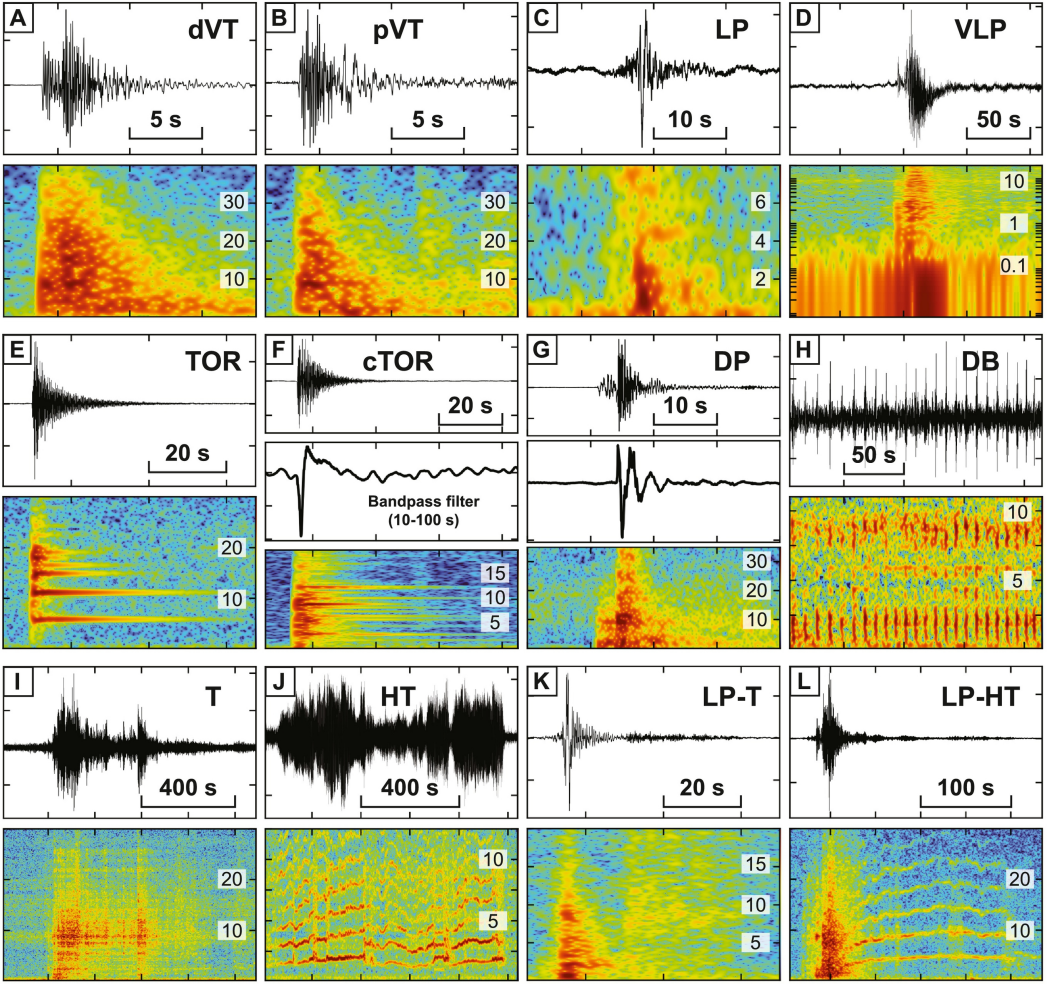
A
dVT
5 s
30
20
10
B
pVT
5 s
30
20
10
C
LP
10 s
6
4
2
D
VLP
50 s
10
1
0.1
E
TOR
20 s
20
10
F
cTOR
20 s
Bandpass filter
(10-100 s)
15
10
5
G
DP
10 s
30
20
10
H
DB
50 s
10
5
I
T
400 s
20
10
J
HT
400 s
10
5
K
LP-T
20 s
15
10
5
L
LP-HT
100 s
20
10

Figure 6

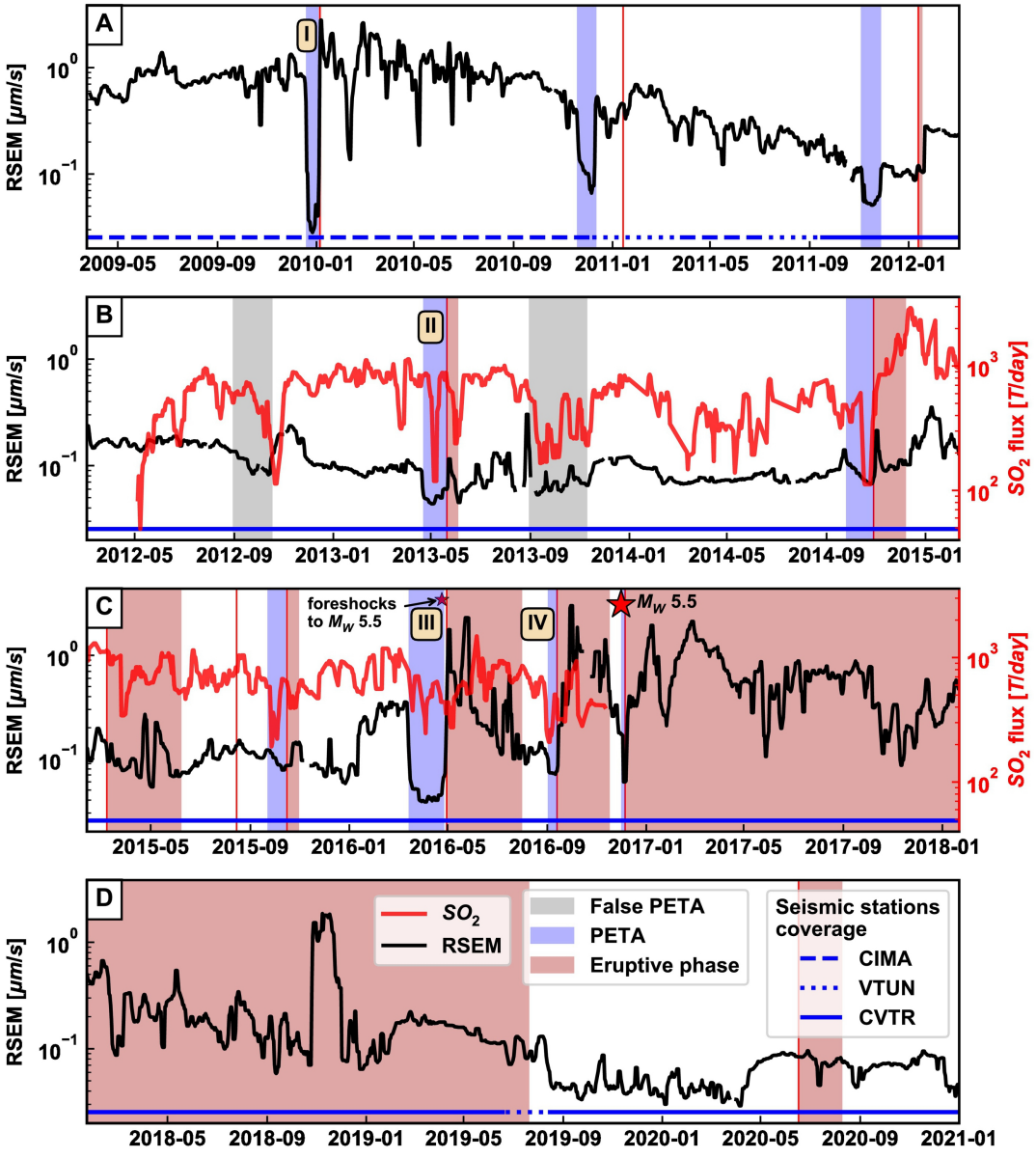
A
I
RSEM [μm/s]
10^0
10^{-1}
2009-05
2009-09
2010-01
2010-05
2010-09
2011-01
2011-05
2011-09
2012-01
B
II
RSEM [μm/s]
SO_2 flux [T/day]
10^3
10^2
2012-05
2012-09
2013-01
2013-05
2013-09
2014-01
2014-05
2014-09
2015-01
C
foreshocks to M_W 5.5
III
IV
M_W 5.5
RSEM [μm/s]
SO_2 flux [T/day]
2015-05
2015-09
2016-01
2016-05
2016-09
2017-01
2017-05
2017-09
2018-01
D
SO_2
RSEM
False PETA
PETA
Eruptive phase
Seismic stations coverage
CIMA
VTUN
CVTR
RSEM [μm/s]
2018-05
2018-09
2019-01
2019-05
2019-09
2020-01
2020-05
2020-09
2021-01

Figure 7

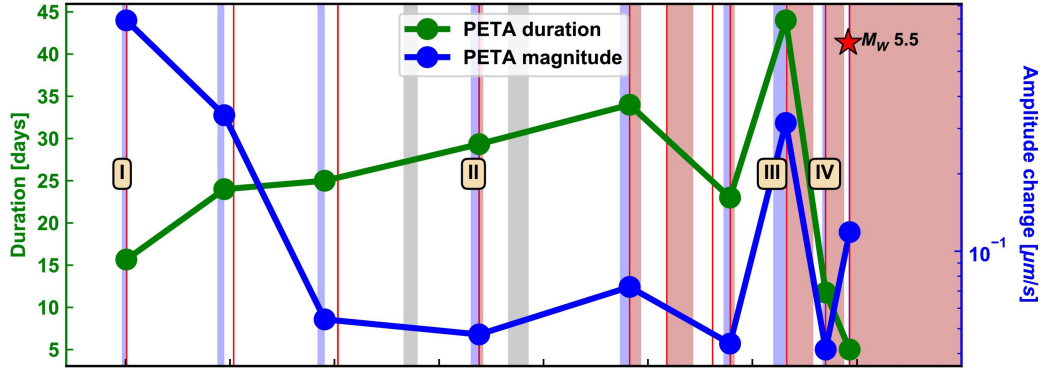
PETA duration
PETA magnitude
M_W 5.5
I
II
III
IV
Duration [days]
Amplitude change [$\mu m/s$]
10^{-1}
45
40
35
30
25
20
15
10
5
2010
2011
2012
2013
2014
2015
2016
2017
2018

Figure 8

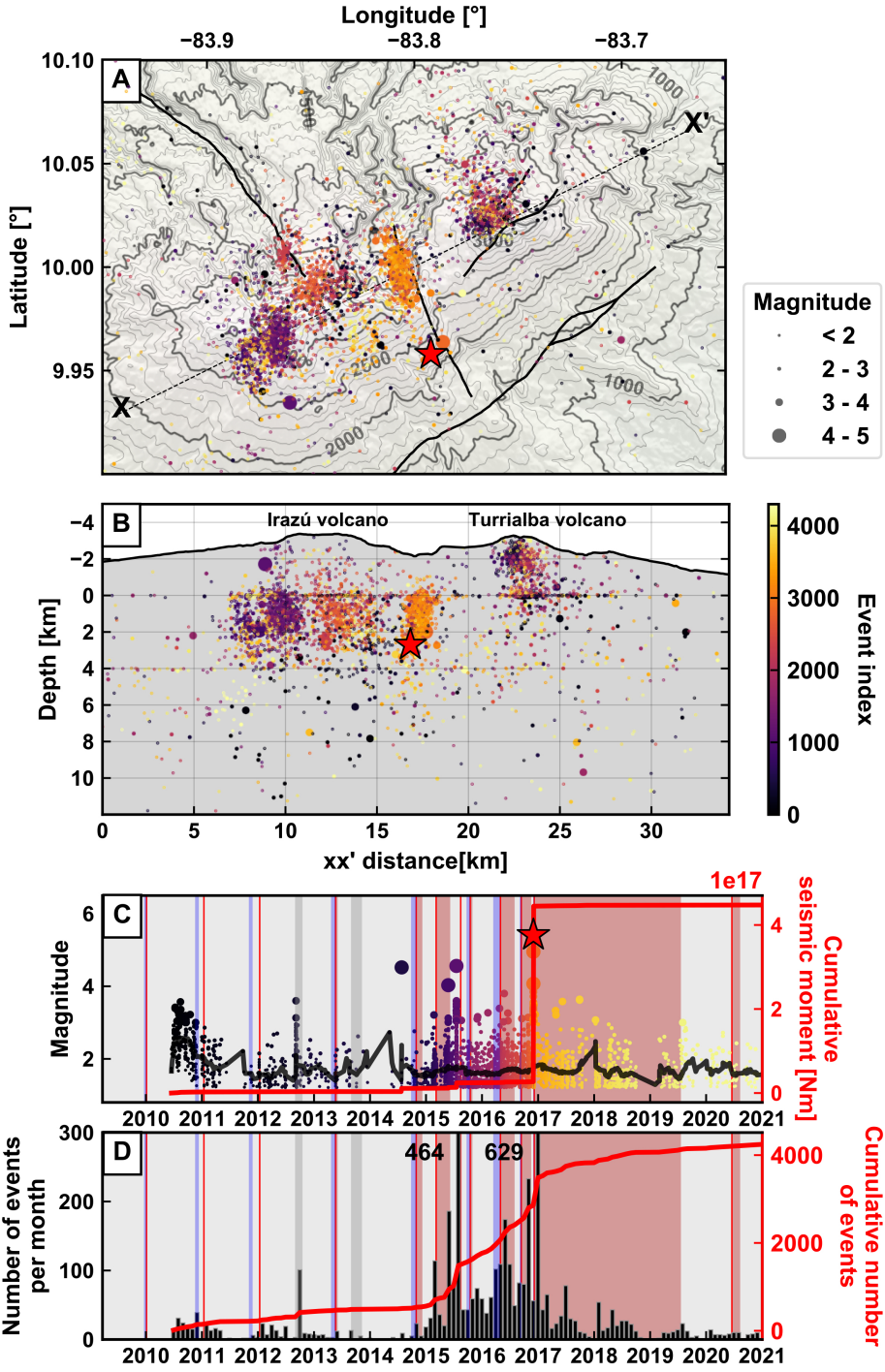
A
Longitude [°]
−83.9
−83.8
−83.7
10.10
10.05
10.00
9.95
Latitude [°]
X
X'
1000
2000
2500
3000
Magnitude
< 2
2 - 3
3 - 4
4 - 5
B
Irazú volcano
Turrialba volcano
Depth [km]
xx' distance[km]
Event index
4000
3000
2000
1000
0
C
Magnitude
1e17
Cumulative seismic moment [Nm]
D
464
629
Number of events per month
Cumulative number of events
2010
2011
2012
2013
2014
2015
2016
2017
2018
2019
2020
2021

Figure 9

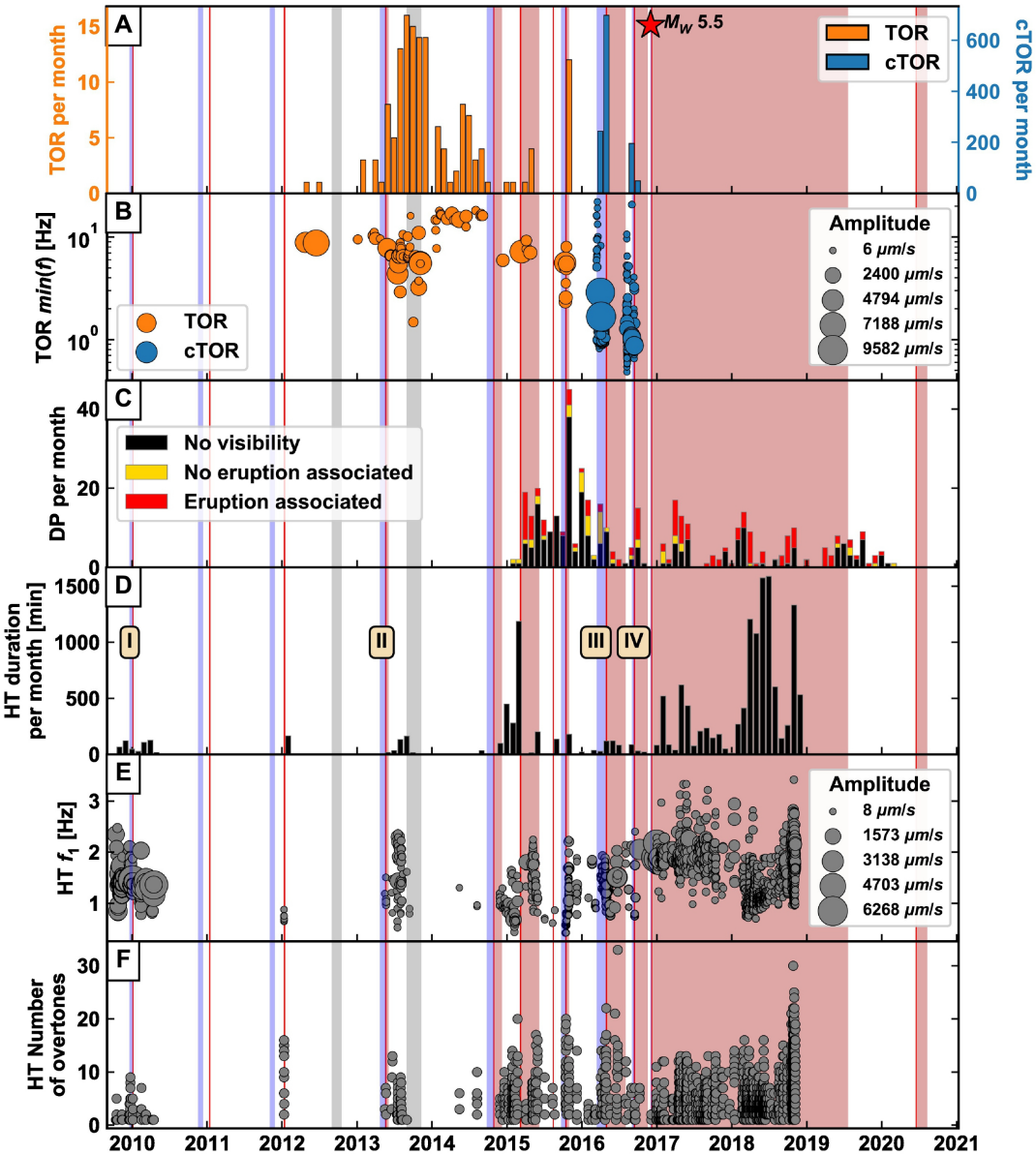
A
TOR per month
cTOR per month
M_W 5.5
TOR
cTOR
B
TOR min(f) [Hz]
TOR
cTOR
Amplitude
6 μm/s
2400 μm/s
4794 μm/s
7188 μm/s
9582 μm/s
C
DP per month
No visibility
No eruption associated
Eruption associated
D
HT duration per month [min]
I
II
III
IV
E
HT f_1 [Hz]
Amplitude
8 μm/s
1573 μm/s
3138 μm/s
4703 μm/s
6268 μm/s
F
HT Number of overtones
2010
2011
2012
2013
2014
2015
2016
2017
2018
2019
2020
2021

Figure 10

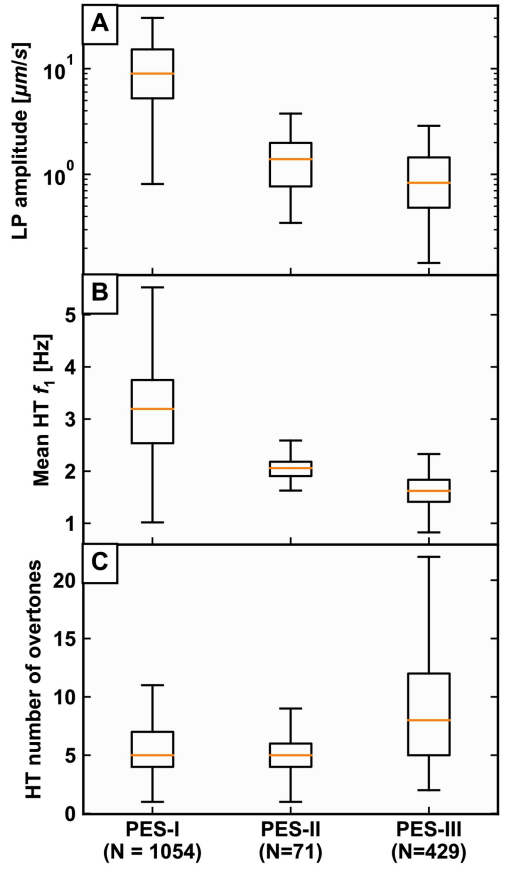
A
LP amplitude [μm/s]
10^1
10^0
B
Mean HT f1 [Hz]
5
4
3
2
1
C
HT number of overtones
20
15
10
5
0
PES-I
(N = 1054)
PES-II
(N=71)
PES-III
(N=429)

Figure 11

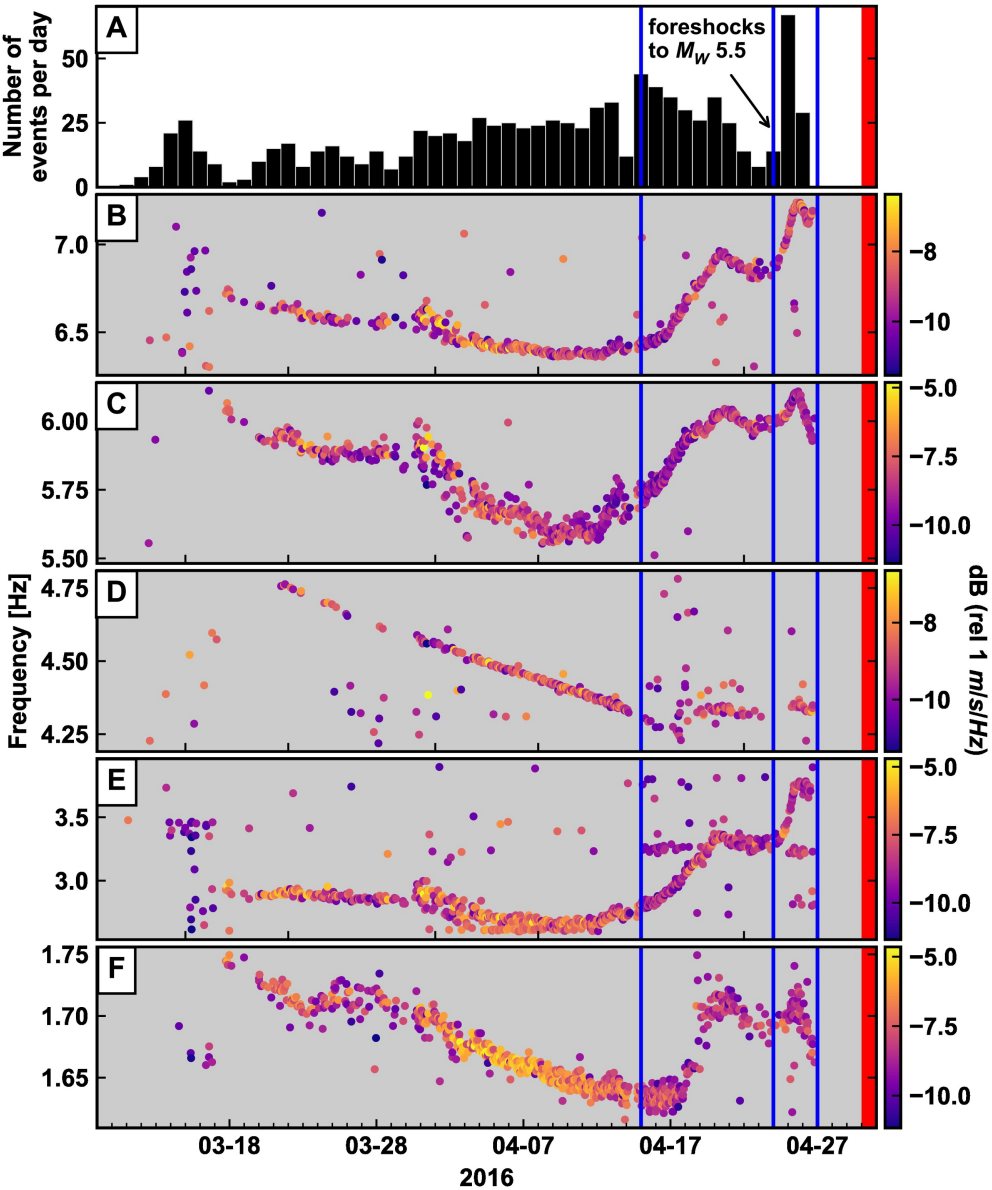
A
Number of events per day
50
25
0
foreshocks to M_W 5.5
B
7.0
6.5
C
6.00
5.75
5.50
D
4.75
4.50
4.25
E
3.5
3.0
F
1.75
1.70
1.65
Frequency [Hz]
−8
−10
−5.0
−7.5
−10.0
dB (rel 1 m/s/Hz)
03-18
03-28
04-07
04-17
04-27
2016

Figure 12

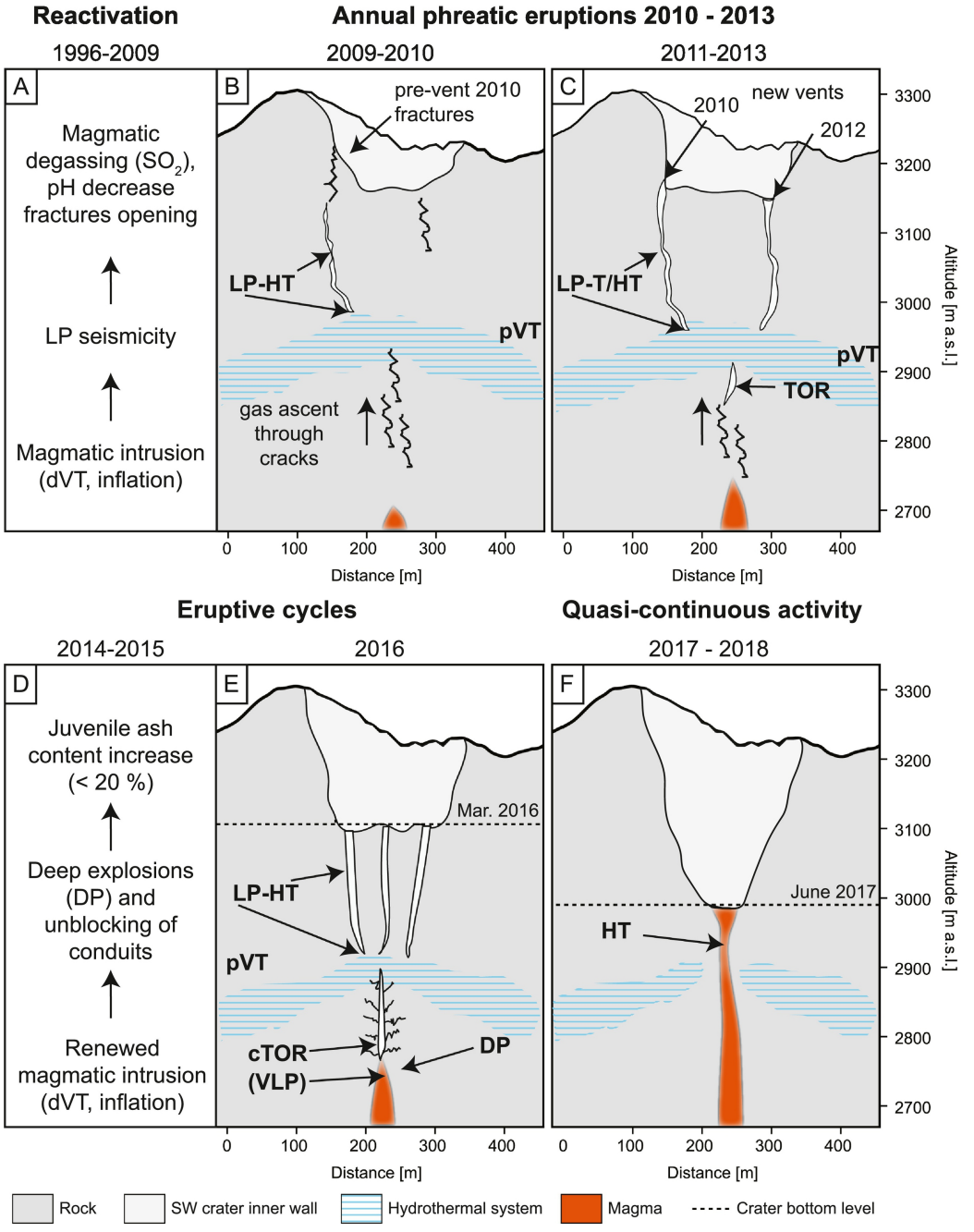
Reactivation
Annual phreatic eruptions 2010 - 2013
1996-2009
2009-2010
2011-2013
A
B
C
Magmatic degassing (SO_2), pH decrease fractures opening
LP seismicity
Magmatic intrusion (dVT, inflation)
pre-vent 2010 fractures
LP-HT
pVT
gas ascent through cracks
2010
new vents
2012
LP-T/HT
pVT
TOR
Altitude [m a.s.l.]
3300
3200
3100
3000
2900
2800
2700
0
100
200
300
400
Distance [m]
Eruptive cycles
Quasi-continuous activity
2014-2015
2016
2017 - 2018
D
E
F
Juvenile ash content increase (< 20 %)
Deep explosions (DP) and unblocking of conduits
Renewed magmatic intrusion (dVT, inflation)
Mar. 2016
LP-HT
pVT
cTOR
(VLP)
DP
June 2017
HT
Rock
SW crater inner wall
Hydrothermal system
Magma
Crater bottom level

Figure 13